# Analysis Procedures for Evaluating Superheavy Load Movement on Flexible Pavements, Volume VIII: Appendix G: Risk Analysis of Buried Utilities Under Superheavy Load Vehicle Movements

PUBLICATION NO. FHWA-HRT-18-056

OCTOBER 2019

U.S. Department of Transportation
**Federal Highway Administration**

Research, Development, and Technology
Turner-Fairbank Highway Research Center
6300 Georgetown Pike
McLean, VA 22101-2296

## FOREWORD

The movement of superheavy loads (SHLs) on the Nation's highways is an increasingly common, vital economic necessity for many important industries, such as chemical, oil, electrical, and defense. Many superheavy components are extremely large and heavy (gross vehicle weights in excess of a few million pounds), and they often require specialized trailers and hauling units. At times, SHL vehicles have been assembled to suit the load being transported, and therefore, the axle configurations have not been standard or consistent. Accommodating SHL movements without undue damage to highway infrastructure requires the determination of whether the pavement is structurally adequate to sustain the SHL movement and protect any underground utilities. Such determination involves analyzing the likelihood of instantaneous or rapid load-induced shear failure of the pavement structure.

The goal of this project was to develop a comprehensive analysis process for evaluating SHL movement on flexible pavements. As part of this project, a comprehensive mechanistic-based analysis approach consisting of several analysis procedures was developed for flexible pavement structures and documented in a 10-volume series of Federal Highway Administration reports—a final report and 9 appendices.[1–9] This is *Analysis Procedures for Evaluating Superheavy Load Movement on Flexible Pavements, Volume VIII: Appendix G, Risk Analysis of Buried Utilities Under SHL Vehicle Movements*, and it details the analysis procedures to investigate flexible and rigid buried utilities failure risks under SHL-vehicle movements. It also verifies the proposed approach using large-scale experiments on full-scale pavement structures. This report is intended for use by highway agency pavement engineers responsible for assessing the structural adequacy of pavements in the proposed route and identifying mitigation strategies, where warranted, in support of the agency's response to SHL-movement permit requests.

Cheryl Allen Richter, Ph.D., P.E.
Director, Office of Infrastructure
Research and Development

# TECHNICAL REPORT DOCUMENTATION PAGE

| 1. Report No.<br>FHWA-HRT-18-056 | 2. Government Accession No. | 3. Recipient's Catalog No. |
|---|---|---|
| 4. Title and Subtitle<br>Analysis Procedures for Evaluating Superheavy Load Movement on Flexible Pavements, Volume VIII: Appendix G, Risk Analysis of Buried Utilities Under Superheavy Load Vehicle Movements | | 5. Report Date<br>August 2019<br>6. Performing Organization Code |
| 7. Author(s)<br>Hadi Nabizadeh (ORCID: 0000-0001-8215-1299),<br>Sherif Elfass (ORCID: 0000-0003-3401-6513),<br>Elie Y. Hajj (ORCID: 0000-0001-8568-6360),<br>Raj V. Siddharthan (ORCID: 0000-0002-3847-7934),<br>Mohamed Nimeri (ORCID: 0000-0002-3328-4367), and<br>Murugaiyah Piratheepan (ORCID: 0000-0002-3302-4856) | | 8. Performing Organization Report No.<br>WRSC-UNR-201710-01G |
| 9. Performing Organization Name and Address<br>Department of Civil and Environmental Engineering<br>University of Nevada<br>1664 North Virginia Street<br>Reno, NV 89557 | | 10. Work Unit No.<br>11. Contract or Grant No.<br>DTFH61-13-C-00014 |
| 12. Sponsoring Agency Name and Address<br>Office of Infrastructure Research and Development<br>Federal Highway Administration<br>Turner-Fairbank Highway Research Center<br>6300 Georgetown Pike<br>McLean, VA 22101 | | 13. Type of Report and Period Covered<br>Final Report; August 2013–July 2018<br>14. Sponsoring Agency Code<br>HRDI-20 |
| 15. Supplementary Notes<br>Nadarajah Sivaneswaran (HRDI-20; ORCID: 0000-0003-0287-664X), Office of Infrastructure Research and Development, Turner-Fairbank Highway Research Center, served as the Contracting Officer's Representative. | | |


16. Abstract

The movement of superheavy loads (SHLs) has become more common over the years since it is a vital necessity for many important industries, such as chemical, oil, electrical, and defense. SHL hauling units are much larger in size and weight compared to the standard trucks. SHL gross vehicle weights may be in excess of a few million pounds, so they often require specialized trailers and components with nonstandard spacing between tires and axles. Accommodating SHL-vehicle movements requires the determination of whether the pavement is structurally adequate and involves the analysis of the likelihood of instantaneous or rapid load-induced shear failure. As part of the Federal Highway Administration project, Analysis Procedures for Evaluating Superheavy Load Movement on Flexible Pavements, methods for conducting buried utilities risk analyses in a flexible pavement under SHL-vehicle movements were developed. The available and widely accepted state-of-practice procedures to examine the structural integrity of flexible and rigid buried utilities subjected to standard traffic live load were adopted in this project. However, significant shortfalls in the existing methodologies, such as the impact of the layered nature of the existing flexible pavement, the role of unconventional surface loading from an SHL vehicle, and the effect of vehicle speed, were addressed by the use of 3D-Move Analysis software.[(10)] To account for the existence of buried utilities in 3D-Move Analysis, computed SHL vehicle–induced stresses were modified using a stress adjustment factor for buried utilities ($SAF_{Utility}$). $SAF_{Utility}$ was determined based on results from large-scale pavement experiments conducted in this study.


| 17. Key Words | 18. Distribution Statement |
|---|---|
| Superheavy load, flexible pavement, large-scale testing, instrumentation, flexible pipes, rigid culverts | No restrictions. This document is available through the National Technical Information Service, Springfield, VA 22161.<br>http://www.ntis.gov |

| 19. Security Classif. (of this report) | 20. Security Classif. (of this page) | 21. No. of Pages | 22. Price |
|---|---|---|---|
| Unclassified | Unclassified | 67 | N/A |

# SI* (MODERN METRIC) CONVERSION FACTORS

## APPROXIMATE CONVERSIONS TO SI UNITS

| Symbol | When You Know | Multiply By | To Find | Symbol |
|---|---|---|---|---|
| | | **LENGTH** | | |
| in | inches | 25.4 | millimeters | mm |
| ft | feet | 0.305 | meters | m |
| yd | yards | 0.914 | meters | m |
| mi | miles | 1.61 | kilometers | km |
| | | **AREA** | | |
| $in^2$ | square inches | 645.2 | square millimeters | $mm^2$ |
| $ft^2$ | square feet | 0.093 | square meters | $m^2$ |
| $yd^2$ | square yard | 0.836 | square meters | $m^2$ |
| ac | acres | 0.405 | hectares | ha |
| $mi^2$ | square miles | 2.59 | square kilometers | $km^2$ |
| | | **VOLUME** | | |
| fl oz | fluid ounces | 29.57 | milliliters | mL |
| gal | gallons | 3.785 | liters | L |
| $ft^3$ | cubic feet | 0.028 | cubic meters | $m^3$ |
| $yd^3$ | cubic yards | 0.765 | cubic meters | $m^3$ |
| | NOTE: volumes greater than 1000 L shall be shown in $m^3$ | | | |
| | | **MASS** | | |
| oz | ounces | 28.35 | grams | g |
| lb | pounds | 0.454 | kilograms | kg |
| T | short tons (2000 lb) | 0.907 | megagrams (or "metric ton") | Mg (or "t") |
| | | **TEMPERATURE (exact degrees)** | | |
| °F | Fahrenheit | 5 (F-32)/9<br>or (F-32)/1.8 | Celsius | °C |
| | | **ILLUMINATION** | | |
| fc | foot-candles | 10.76 | lux | lx |
| fl | foot-Lamberts | 3.426 | $candela/m^2$ | $cd/m^2$ |
| | | **FORCE and PRESSURE or STRESS** | | |
| lbf | poundforce | 4.45 | newtons | N |
| $lbf/in^2$ | poundforce per square inch | 6.89 | kilopascals | kPa |

## APPROXIMATE CONVERSIONS FROM SI UNITS

| Symbol | When You Know | Multiply By | To Find | Symbol |
|---|---|---|---|---|
| | | **LENGTH** | | |
| mm | millimeters | 0.039 | inches | in |
| m | meters | 3.28 | feet | ft |
| m | meters | 1.09 | yards | yd |
| km | kilometers | 0.621 | miles | mi |
| | | **AREA** | | |
| $mm^2$ | square millimeters | 0.0016 | square inches | $in^2$ |
| $m^2$ | square meters | 10.764 | square feet | $ft^2$ |
| $m^2$ | square meters | 1.195 | square yards | $yd^2$ |
| ha | hectares | 2.47 | acres | ac |
| $km^2$ | square kilometers | 0.386 | square miles | $mi^2$ |
| | | **VOLUME** | | |
| mL | milliliters | 0.034 | fluid ounces | fl oz |
| L | liters | 0.264 | gallons | gal |
| $m^3$ | cubic meters | 35.314 | cubic feet | $ft^3$ |
| $m^3$ | cubic meters | 1.307 | cubic yards | $yd^3$ |
| | | **MASS** | | |
| g | grams | 0.035 | ounces | oz |
| kg | kilograms | 2.202 | pounds | lb |
| Mg (or "t") | megagrams (or "metric ton") | 1.103 | short tons (2000 lb) | T |
| | | **TEMPERATURE (exact degrees)** | | |
| °C | Celsius | 1.8C+32 | Fahrenheit | °F |
| | | **ILLUMINATION** | | |
| lx | lux | 0.0929 | foot-candles | fc |
| $cd/m^2$ | $candela/m^2$ | 0.2919 | foot-Lamberts | fl |
| | | **FORCE and PRESSURE or STRESS** | | |
| N | newtons | 0.225 | poundforce | lbf |
| kPa | kilopascals | 0.145 | poundforce per square inch | $lbf/in^2$ |

*SI is the symbol for the International System of Units. Appropriate rounding should be made to comply with Section 4 of ASTM E380.
(Revised March 2003)

## ANALYSIS PROCEDURES FOR EVALUATING SUPERHEAVY LOAD MOVEMENT ON FLEXIBLE PAVEMENTS PROJECT REPORT SERIES

This volume is the eighth of 10 volumes in this research report series. Volume I is the final report, and Volume II through Volume X consist of Appendix A through Appendix I. Any reference to a volume in this series will be referenced in the text as "Volume II: Appendix A," "Volume III: Appendix B," and so forth. The following list contains the volumes:

| Volume | Title | Report Number |
|---|---|---|
| I | Analysis Procedures for Evaluating Superheavy Load Movement on Flexible Pavements, Volume I: Final Report | FHWA-HRT-18-049 |
| II | Analysis Procedures for Evaluating Superheavy Load Movement on Flexible Pavements, Volume II: Appendix A, Experimental Program | FHWA-HRT-18-050 |
| III | Analysis Procedures for Evaluating Superheavy Load Movement on Flexible Pavements, Volume III: Appendix B, Superheavy Load Configurations and Nucleus of Analysis Vehicle | FHWA-HRT-18-051 |
| IV | Analysis Procedures for Evaluating Superheavy Load Movement on Flexible Pavements, Volume IV: Appendix C, Material Characterization for Superheavy Load Movement Analysis | FHWA-HRT-18-052 |
| V | Analysis Procedures for Evaluating Superheavy Load Movement on Flexible Pavements, Volume V: Appendix D, Estimation of Subgrade Shear Strength Parameters Using Falling Weight Deflectometer | FHWA-HRT-18-053 |
| VI | Analysis Procedures for Evaluating Superheavy Load Movement on Flexible Pavements, Volume VI: Appendix E, Ultimate and Service Limit Analyses | FHWA-HRT-18-054 |
| VII | Analysis Procedures for Evaluating Superheavy Load Movement on Flexible Pavements, Volume VII: Appendix F, Failure Analysis of Sloped Pavement Shoulders | FHWA-HRT-18-055 |
| VIII | Analysis Procedures for Evaluating Superheavy Load Movement on Flexible Pavements, Volume VIII: Appendix G, Risk Analysis of Buried Utilities Under Superheavy Load Vehicle Movements | FHWA-HRT-18-056 |
| IX | Analysis Procedures for Evaluating Superheavy Load Movement on Flexible Pavements, Volume IX: Appendix H, Analysis of Cost Allocation Associated with Pavement Damage Under a Superheavy Load Vehicle Movement | FHWA-HRT-18-057 |
| X | Analysis Procedures for Evaluating Superheavy Load Movement on Flexible Pavements, Volume X: Appendix I, Analysis Package for Superheavy Load Vehicle Movement on Flexible Pavement (SuperPACK) | FHWA-HRT-18-058 |

## TABLE OF CONTENTS

## LIST OF FIGURES

## LIST OF TABLES

## LIST OF ABBREVIATIONS AND SYMBOLS

### Abbreviations

| | |
|---|---|
| 3D | three-dimensional |
| AASHTO | American Association of State Highway and Transportation Officials |
| AC | asphalt concrete |
| ALA | American Lifelines Alliance |
| API | American Petroleum Institute |
| CAB | crushed aggregate base |
| CEPA | Canadian Energy Pipeline Association |
| FHWA | Federal Highway Administration |
| FWD | falling weight deflectometer |
| HDPE | high-density polyethylene |
| LVDT | linear variable differential transformer |
| PVC | polyvinyl chloride |
| SG | subgrade |
| SHL | superheavy load |
| TEPC | total earth pressure cell |

### Symbols

| | |
|---|---|
| $A_g$ | gross area of a section |
| $A_s$ | available reinforcement area |
| $b$ | strip width |
| $B'$ | coefficient of elastic support |
| $B_{culvert}$ | width of the culvert |
| $B_{trench}$ | width of the trench |
| $C_d$ | load coefficient for soil–structure interaction factor |
| $Cover$ | concrete cover on the reinforcements |
| $d_e$ | effective depth |
| $D_l$ | deflection lag factor |
| $D_{Reinforcement}$ | diameter of the longitudinal reinforcements |
| $d_v$ | effective shear depth |
| $E'$ | modulus of soil reaction |
| $E_{pipe}$ | modulus of elasticity of the pipe |
| $f'_c$ | compressive strength of the concrete |
| $F_e$ | soil–structure interaction factor |
| $FOS_{CSF}$ | factor of safety against the pipe circumferential stress failure |
| $FOS_{wc}$ | factor of safety against wall-crushing stress |
| $FS_{req}$ | required factor of safety for ring-buckling stress |
| $f_y$ | yield strength of the reinforcement |
| $h_{cover}$ | depth to the top of the pipe |
| $H_{culvert}$ | embedment depth of the culvert from the surface |
| $h_w$ | height of the water surface above the top of the pipe |
| $I_{pipe}$ | moment of inertia of the pipe wall cross section per inch of pipe |

| | |
|---|---|
| $K_b$ | bedding constant. |
| $K_B$ | bending moment parameter |
| $K_Z$ | deflection parameter |
| $K\mu'$ | constant parameter as function of soil type |
| $l_{culvert}$ | length of culvert opening |
| $l_t$ | tire length |
| $Load_{SHL}$ | load distribution on top of the box culvert resulting from a superheavy load vehicle |
| $M_n$ | flexural resistance |
| $M_u$ | maximum induced moment |
| $OD_{pipe}$ | outer diameter of a pipe |
| $P_{int}$ | pipe internal pressure |
| $Pipe_{ovality}$ | pipe ovality |
| $P_n$ | compressive axial resistance |
| $P_p$ | vertical stress due to live load |
| $P_u$ | axial thrust |
| $P_v$ | vertical stress due to dead load |
| $R_W$ | water buoyancy factor |
| $SAF_{Utility}$ | stress adjustment factor for buried utilities |
| $SAF_{Flexible}$ | stress adjustment factor for a flexible pipe |
| $SAF_{Rigid}$ | stress adjustment factor for a rigid culvert |
| $S_{hi}$ | pipe circumferential stress due to internal pressure |
| $SMYS$ | specified minimum yield strength of pipe material |
| $S_{shear}$ | spacing of shear reinforcement |
| $t_{culvert}$ | thickness of a culvert member |
| $t_{pipe}$ | thickness of the pipe wall |
| $T_{pw}$ | thrust in the pipe wall |
| $V_c$ | nominal shear strength of the concrete |
| $V_n$ | shear resistance |
| $V_u$ | maximum induced shear |
| $w_t$ | tire width |
| $W_{vertical}$ | vertical load due to external loads (dead and live loads) |
| $\phi_a$ | strength reduction factor for compression |
| $\phi_{aPn}$ | factored compressive axial resistance |
| $\phi_f$ | strength reduction factor for flexure |
| $\phi_f M_n$ | factored flexural resistance |
| $\phi_s$ | strength reduction factor for shear |
| $\phi_s V_n$ | factored shear resistance |
| $\Delta y$ | vertical deflection in a pipe cross section |
| $\gamma_{water}$ | unit weight of water |
| $\sigma_0$ | overburden pressure |
| $\sigma_{bw}$ | circumferential stress due to external loads (dead and live loads) |
| $\sigma_{bw\_total}$ | total circumferential stress due to internal pressure and external loads |
| $\sigma_{crb}$ | ring-buckling stress |
| $\sigma_{wc}$ | wall-crushing stress |
| $\sigma_{zz\text{-}3D\text{-}Move}$ | 3D-Move calculated vertical stress |

# CHAPTER 1. INTRODUCTION

Many industries, such as chemical, oil, electrical, and defense, require the movement of superheavy loads (SHLs) on the Nation's highways. SHL hauling units are much larger in size and weight than standard trucks, often with gross vehicle weights in excess of a few million pounds. Accordingly, SHL vehicles frequently necessitate specialized trailers and components with nonstandard spacing between tires and axles. Accommodating SHL-vehicle movements requires determining whether a pavement is structurally adequate and analyzing the likelihood of instantaneous or rapid load-induced shear failure. Figure 1 shows the flowchart of the overall approach developed as part of this Federal Highway Administration (FHWA) project, Analysis Procedures for Evaluating Superheavy Load Movement on Flexible Pavements. In general, the approach consists of the following four major components:

- Ultimate failure analyses.
- Buried utility risk analysis.
- Service limit analyses.
- Cost allocation analysis.

Mitigation strategies may be needed at any stage of the evaluation process when the calculated results fail to meet the respective requirements imposed (e.g., when results indicate a high potential for shear failure of the pavement or damage to buried utilities).

As shown in figure 1, the first step of this approach involves a risk analysis of instantaneous or rapid load-induced ultimate shear failure. Subgrade (SG) is generally the weakest layer in a pavement structure. Thus, a bearing failure analysis should be performed to investigate the likelihood of general bearing capacity failure under an SHL vehicle within the influenced zone of an SG layer. Sloped-shoulder failure analysis, which examines the bearing capacity failure and edge-slope stability associated with a sloped ground under an SHL-vehicle movement, would be the next step. If the ultimate failure analyses reveal no failure in the sloped shoulder, a buried utility risk analysis should be conducted (when applicable). In this analysis, induced stresses and deflections by an SHL vehicle on existing buried utilities are evaluated and compared to established design criteria. Subsequently, if no mitigation strategies are needed, service limit analyses for localized shear failure and deflection-based service limits should be conducted. A localized shear failure analysis is performed to investigate the possibility of failure at the critical location on top of an SG layer under an SHL vehicle. A deflection-based service limit analysis assesses the magnitude of load-induced pavement deflections during an SHL-vehicle movement. This analysis, for instance, may suggest the need for mitigation strategies to meet the imposed acceptable surface-deflection limits. After successfully completing all previously described analyses (i.e., ultimate failure analyses, buried utility risk analysis, and service limit analyses), a cost allocation analysis is conducted.

A summary of the various analysis procedures developed in this study and the associated objectives (including related volume numbers) are summarized in table 1. This report (Volume VIII: Appendix G) is the eighth of 10 volumes and presents the risk analysis of buried utilities in flexible pavements under an SHL-vehicle movement.

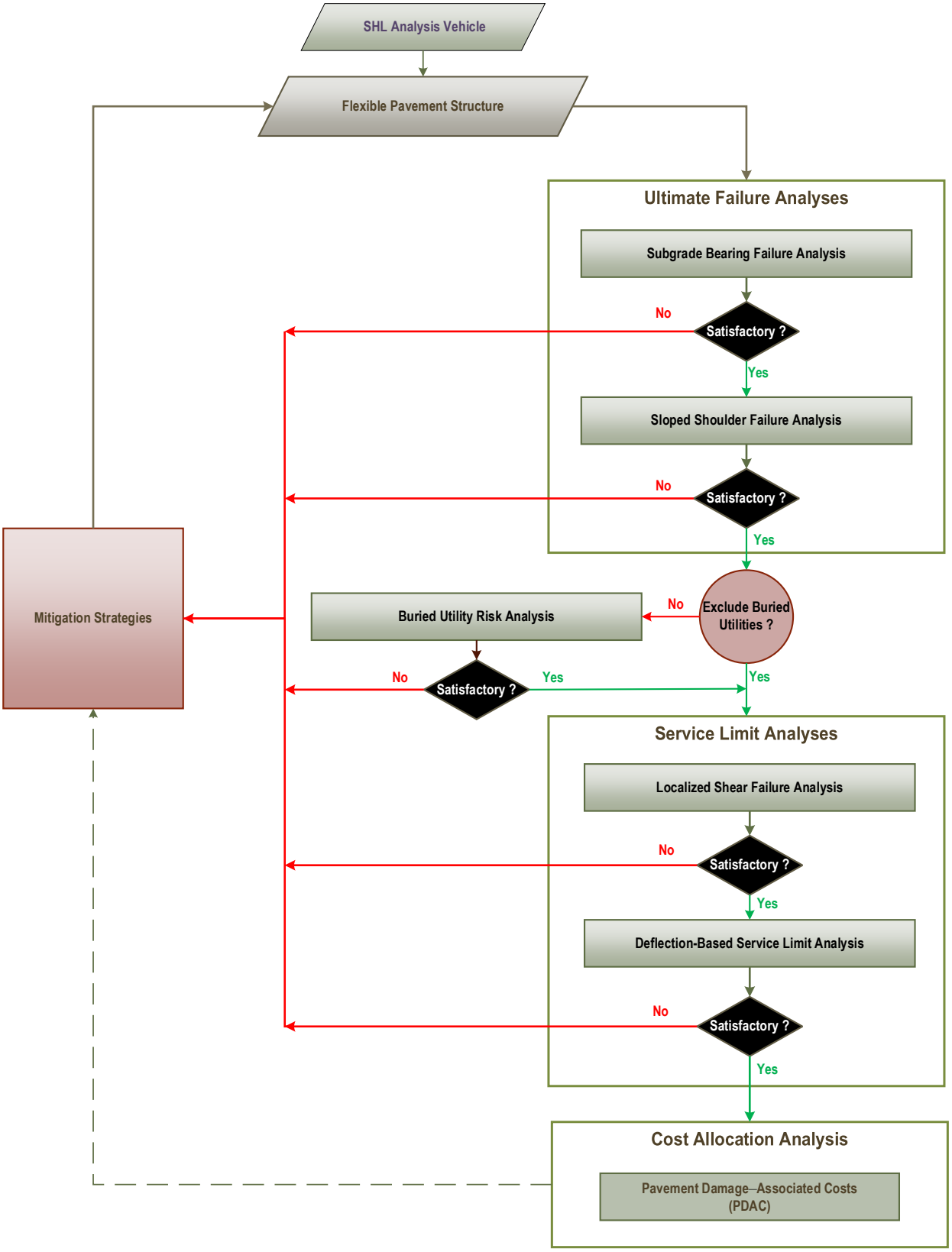




**Figure 1. Flowchart. Overall SHL-vehicle analysis methodology.**

**Table 1. Developed analysis procedures to evaluate SHL movement on flexible pavements.**

| Procedure | Objective |
|---|---|
| SHL analysis vehicle | Identify segment(s) of the SHL vehicle configuration that can be regarded as representative of the entire SHL vehicle (Volume III: Appendix B)[3] |
| Flexible pavement structure | Characterize representative material properties for existing pavement layers (Volume IV: Appendix C and Volume V: Appendix D)[4,5] |
| SG bearing failure analysis | Investigate instantaneous ultimate shear failure in pavement SG (Volume VI: Appendix E)[6] |
| Sloped-shoulder failure analysis | Examine the stability of sloped pavement shoulders under SHL-vehicle movement (Volume VII: Appendix F)[7] |
| Buried utility risk analysis | Perform risk analysis of existing buried utilities (Volume VIII: Appendix G) |
| Localized shear failure analysis | Inspect the likelihood of localized failure (yield) in the pavement SG (Volume VI: Appendix E)[6] |
| Deflection-based service limit analysis | Investigate the development of premature surface distresses (Volume VI: Appendix E)[6] |
| Cost allocation analysis | Determine pavement damage–associated cost attributable to SHL-vehicle movement (Volume IX: Appendix H)[8] |

## 1.1 BACKGROUND

As part of this FHWA project, a study was carried out to assess the risk of buried utilities failure under SHL-vehicle movements. Existing state-of-practice methods that are currently employed for the design of buried utilities were reviewed. While every utility has certain specific design considerations, two common steps are being followed in the existing design methods. In the first step, the load distribution on the buried utility structure due to the dead (i.e., soil overburden) and live (i.e., traffic) loads is determined. Well-established common practices to accomplish the first step are available. Subsequently, in step 2, the buried utility structure is designed in accordance with the specification unique to its type. The internal integrity of an existing utility subjected to the dead and live loads is assessed, as detailed in chapter 2. Since step 2 of analyzing any buried utility is well established, the focus of this FHWA study was on the available methods for step 1.

Typical underground utilities that are often found near highway routes include sewer lines, drain lines, water mains, gas lines, telephone and electrical conduits, culverts, oil and coal slurry lines, and heat distribution lines.[11] Buried utilities are expected to withstand the live and dead load-induced stresses during their expected service life of about 50 to 100 yr. The critical factors that govern the performance of buried utilities are backfill and its compaction, type of buried utility, depth of cover, and external loads.

In general, underground utility structures are categorized as flexible or rigid. A flexible pipe should be able to withstand at least a 2 percent deflection ratio (i.e., vertical deflection normalized with respect to the original size) without any significant structural distresses. The

utility structures that do not meet this criterion are generally considered rigid.[11] Steel, ductile or cast iron, and plastic pipes—which are more ductile—are usually classified as flexible. Concrete and clay pipes are usually considered rigid. Stiffness in flexible pipes is an important factor in resisting failure modes, such as ring deflection or buckling. On the other hand, rigid utilities should be designed to resist wall stresses resulting from internal pressure and external loads.[11]

The stresses induced on buried utilities from dead (i.e., overburden) and live (i.e., traffic) loads strongly depend on the stiffness properties of the utility and the surrounding soil. This phenomenon is commonly referred to as soil–structure interaction. In rigid utility structures, it is generally assumed that the vertical stresses are more critical, and horizontal stresses are often neglected. On the other hand, the performance of flexible utility structures (e.g., deflection) depends on both the vertical and horizontal stresses due to the surrounding soil reaction.[12]

The Marston theory is routinely used to compute dead loads on rigid utilities.[13] Based on this theory, the resultant load on an underground structure is computed as the weight of the material above the top of the conduit minus the shearing or friction forces along the sides of the trench. Applicability of the Marston theory for determining dead loads on buried flexible pipes was investigated by Spangler, who concluded that this theory is not applicable for a flexible pipe.[14] Accordingly, Spangler incorporated the effects of the surrounding soil and developed the method known as the Iowa formula.

Several experimental and analytical attempts have been made to investigate the stress variation as a function of depth from surface traffic live loads. The classical Boussinesq solution and other solutions, such as spreading the load over an area as a linear function of depth, are the most widely used calculation approaches.[15] As shown in figure 2, applicability of classical solutions is often constrained to linear elastic, homogenous, and half-space soil conditions.

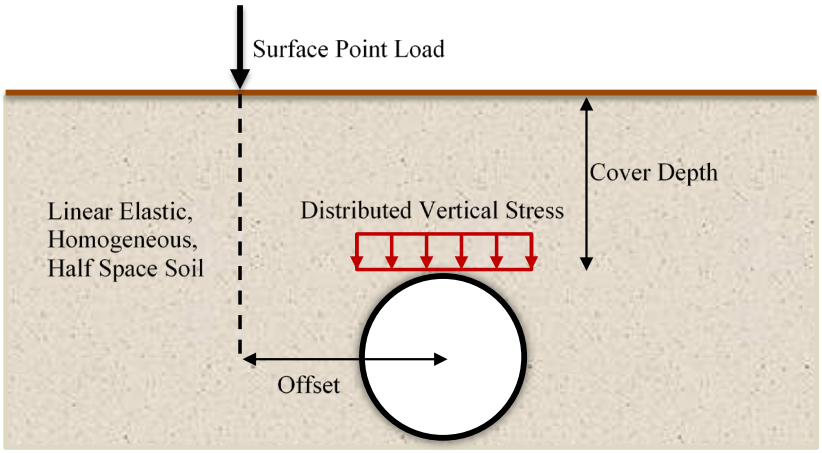




**Figure 2. Illustration. Distributed vertical stress on top of utility based on the Boussinesq solution.**

The most recent American Association of State Highway and Transportation Officials' (AASHTO's) Standard Specification, *Load and Resistance Factor Design Bridge Construction Specifications*, proposes approaches to investigate live-load spreading through homogenous SG soil irrespective of the characteristics of the buried structure (i.e., flexible or rigid).[16] The

AASHTO standard specification recommends applying a live load as a point load at the surface and spreading loads at a rate of 1.75 to the cover depth. Subsequently, the load is increased by 30 percent for zero cover depth and decreased to 0 percent for cover depths of more than 3 ft in order to consider the dynamic load allowance (i.e., impact effects).

On the other hand, the AASHTO standard specification requires that the live load should be applied as a uniform rectangular tire footprint of 10 by 20 inches at the surface but attenuate with a load coefficient (1.00 or 1.15 as a function of soil type) as the depth of the fill increases, as illustrated in figure 3.[16] Dynamic load allowance equal to 33 percent for zero cover depth and 0 percent for depths greater than 8 ft is then applied. It should be mentioned that the AASHTO standard specification considers a live load to be equal to 16,000 lb, which represents an HS20 class loading.[16] Additionally, if the buried utility is located in the wheel interaction depth, both methods double the distributed pressure on top of the utility, as shown in figure 4.

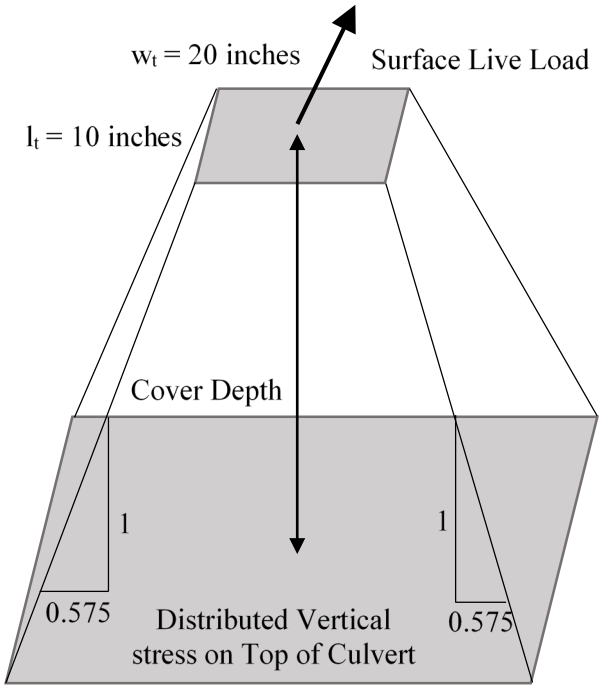




**Figure 3. Illustration. Distributed vertical stress on top of utility based on AASHTO standard specification.**

Where:

$w_t$ = tire width.
$l_t$ = tire length.

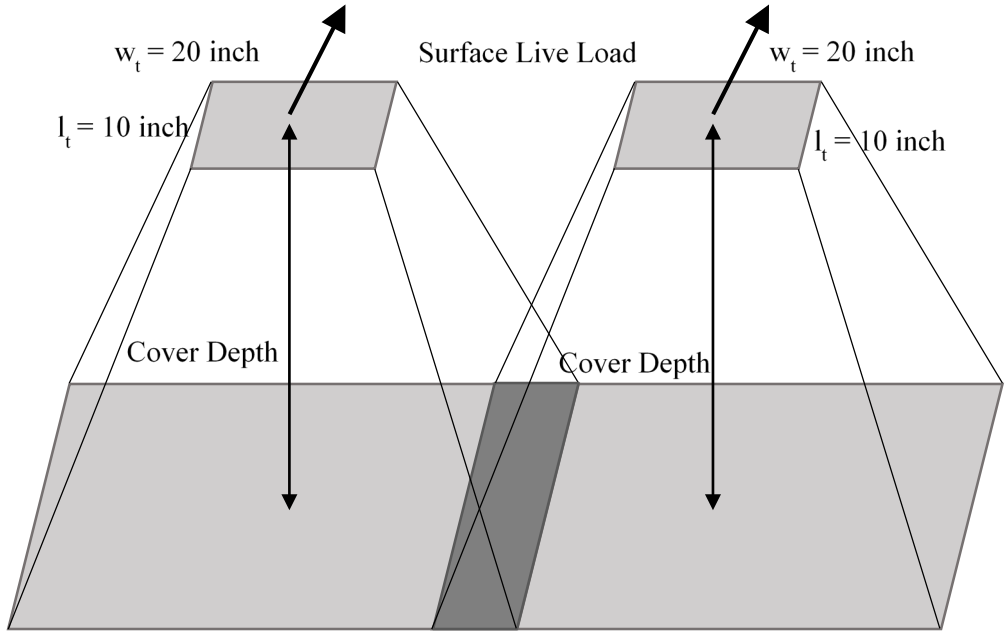



**Figure 4. Illustration. Distributed vertical stress on top of utility based on AASHTO standard specification with interaction from surface loads.**

Previous experimental works have shown that live loads spread over a much greater area than specified by the AASHTO standard specifications.[15–17] Flexible pipes deform under live loads and develop shear stresses in the surrounding soil, which causes the live loads to spread out even further and affect a greater length of pipe. However, in rigid utility structures, the live-load spread mechanism is different. Although rigid utilities do not deform significantly under any load, their high rigidity allows for internal spreading of the load over a greater length of their structure.[15,17]

Petersen et al. investigated the distribution of live loads with depth as a function of soil and culvert types.[15] Three-dimensional (3D) numerical modeling was used while considering the influence of many parameters, such as cover depth, pipe diameter, culvert type, and soil type. As many as 800 3D analyses of buried structures were undertaken. The results show that the aforementioned controlling parameters significantly affected the live-load distribution. The investigators proposed a set of simplified design equations for structural response and live-load distribution as a function of culvert type. In the Petersen et al. study, an HS20 truck live load was simulated and applied on top of the SG without considering the presence of a crushed aggregate base (CAB) or an asphalt concrete (AC) layer.[15]

Kraus et al. conducted numerical and laboratory-based studies to evaluate the impact of overweight loads on buried utilities.[18] Two-dimensional numerical modeling was used to perform sensitivity analysis to evaluate the effects of various parameters on potential damage to buried utilities due to SHL-vehicle movement. Similar to the Peterson et al. study, the investigation in the Kraus et al. study was performed on utilities buried under unpaved roads and static loading conditions.[15,18]

## 1.2 PROBLEM STATEMENT

A fair assessment of the induced stresses from dead and live loads is required to analyze the internal integrity of a buried utility. Although the state of practice uses methods that provide recommendations with respect to the load distribution, they are limited, especially when assessing the risk to buried utilities under an SHL-vehicle movement. The following list contains the limitations of the state of practice:

- **Considering only the standard truck (mostly HS20) as live load and simulating it as a point load or as a rectangular tire footprint (typically 10 by 20 inches):** SHL-hauling units are much larger in size and weight compared to standard trucks. The axle and tire configurations used in the hauling units are different. In other words, the spacing between tires and axles is not standard, and the tire imprints as a whole can span over the entire width of a lane. Consequently, the effects of closely spaced tires, nonuniform tire pressure distribution, and much heavier tire load cannot be addressed directly using the existing methods.

- **Applying surface-tire loads directly at the surface of unpaved roads (i.e., on top of the SG):** This case represents the worst-case scenario since AC and CAB layers affect the stress distribution and can significantly reduce the stresses transferred to the utility. While this may be a good design practice, for a realistic buried utility assessment subjected to an SHL-vehicle movement, the role of existing pavement layers should be addressed.

- **Spreading the live load at a constant rate to the depth of SG soil cover:** This assumption is not valid when considering a multilayer system with distinct stiffness material properties (i.e., flexible pavement structure).

- **Simulating and applying the live load as a static load:** This might be a proper assumption since properties of existing AC layers are not taken into consideration in available methodologies. However, the influence of speed on the viscoelastic behavior of an AC layer needs to be adequately accounted for in the stress distribution estimation process under an SHL-vehicle movement.

It is important to reliably address these limitations for the estimation of SHL vehicle–induced vertical stresses on buried utilities.

## 1.3 OBJECTIVES AND SCOPE OF WORK

Developing a methodology to analyze the failure risk of buried utility structures under an SHL-vehicle movement is one of the key activities of this FHWA study. The buried utilities risk analysis can only be achieved by reliably assessing the increase in stresses due to live load (i.e., step 1 in this analysis) while adopting the existing procedures in assessing the integrity of buried utilities under the SHL vehicle–induced stresses (i.e., step 2 in this analysis). 3D-Move Analysis software was used to simulate pavement structures and to compute the SHL vehicle-induced vertical stresses at the location of buried utilities.[10] However, some limitations in relation to the buried utilities analysis using 3D-Move Analysis software need to be addressed.

3D-Move Analysis software is an efficient dynamic finite-layer–based model that is capable of calculating pavement responses under static and dynamic (i.e., moving) surface loads.[10] The software can account for the viscoelastic properties of the AC layer and the nonuniform tire–pavement interface stresses (normal and shear) on a loaded area of any shape. However, the software assumes that uniform layer stiffness extends laterally to infinity without considering the role of soil–structure interaction and discontinuities within the medium (i.e., existence of buried utilities). Therefore, these aspects need to be accounted for when this software is used to compute SHL vehicle–induced stresses. It may be necessary to modify the 3D-Move Analysis software-computed, load-induced stresses at the location of the buried utility through the implementation of a stress adjustment factor for buried utilities ($SAF_{Utility}$).[10]

In order to determine $SAF_{Utility}$, large-scale experiments comprising a typical pavement structure (i.e., experiments No. 3 and No. 5) were designed and carried out (see section 3.1 for further detail). While pavement structure and materials were similar in these experiments, buried utilities, including one steel pipe and one reinforced concrete square box culvert, were located in the SG of experiment No. 5. The recorded test results and behaviors of buried utilities were scrutinized to determine $SAF_{Utility}$, as described in this report. The adjusted vertical stresses from 3D-Move Analysis software were subsequently incorporated in the adopted methodologies to perform a buried utility assessment.[10]

# CHAPTER 2. PROCEDURES FOR RISK ANALYSIS OF BURIED UTILITIES UNDER SHL-VEHICLE MOVEMENTS

This chapter summarizes the available state-of-practice procedures to examine the structural integrity of flexible and rigid buried utilities subjected to standard traffic live load. Due to the widely accepted nature of these existing procedures, they were adopted in this study to assess the risk to buried utilities under SHL movements. However, as mentioned in chapter 1, significant shortfalls (i.e., the impact of existing flexible pavement, the role of unconventional surface loading from SHL vehicles, and the effect of vehicle speed) need to be addressed when computing the increase in stresses due to surface load in these procedures.

## 2.1. PROCEDURE FOR FLEXIBLE UTILITIES

Flexible pipes are commonly used as buried underground conduits for roadways and highways. A literature review of guidelines in designing flexible pipes and the methodology used in this study are presented in this section.

### 2.1.1 Background

Flexible pipes are usually made of steel, ductile or cast iron, corrugated high-density polyethylene (HDPE), and polyvinyl chloride (PVC). By design, they are required to withstand soil overburden (i.e., dead loads) and surface traffic loads (i.e., live loads), as well as fluctuations in groundwater. The load estimation and structural design of buried corrugated metal pipe and thermoplastic pipe (both PVC and HDPE) are provided in sections 3 and 12 of the AASHTO standard specifications, respectively.[16] Common terminology for a typical pipe is illustrated in figure 5.

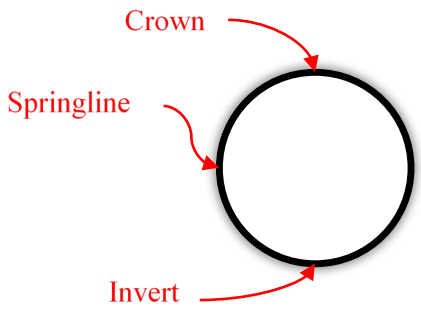




**Figure 5. Illustration. Common terminology for a typical pipe.**

Of the several studies reviewed, two distinct design guidelines presented the most direct benefit to the current project. The first guideline was produced for the American Lifelines Alliance (ALA), *Guidelines for the Design of Buried Steel Pipe* (July 2001 with addenda through February 2005).[19] The purpose of this guideline was to develop design provisions to evaluate the integrity of buried steel pipes for a range of applied loads. One form of the applied loads evaluated was the surface live load. The guidelines cover three specific types of surface live loads: (1) a highway HS20 simulating a 20-T truck traffic load with impact, (2) a railway E80

class loading simulating an 80,000-lb/ft railway load with impact, and (3) an airport simulating an 180,000-lb dual-tandem gear assembly with a 26-inch spacing between tires and a 66-inch center-to-center spacing between fore and aft tires under a 12-inch-thick rigid pavement with impact. Tables as well as equations to evaluate the ovality and stresses exerted on a pipe due to the aforementioned loading conditions for different soil layers are provided in the guidelines.[19] While the guidelines are comprehensive in one area, any guidance on how to assess the stresses induced on steel pipes due to general surface loading (i.e., different load amplitude and configuration) are not presented.

The second study was conducted in 2009 for the Canadian Energy Pipeline Association (CEPA), *Development of a Pipeline Surface Loading Screening Process and Assessment of Surface Load Dispersing Methods*.[20] The motive of the study was the limitations embodied in American Petroleum Institute (API) RP 1102.[21] These limitations are the soil cover depth (must be equal or greater than 3 ft) and surface loads (HS20 with small footprints and tire pressure in excess of 80 psi). The study discusses the methodology for developing a screening tool, which provides a simple "pass/no pass" determination based on attributes such as wheel or axel load, ground surface contact area and/or surface loading pressure, depth of cover, maximum allowable operating pressure, and design factor.[20] According to the study, situations that pass this initial screening would not require any additional analysis, while situations that do not pass the initial screening may need further evaluation. The study also discusses the effectiveness of various temporary or permanent surface load–dispersal and mitigation techniques to lessen the effect of surface loading.[20]

Almost every study that was reviewed referred to the Spangler stress formula and the subsequent Iowa formula. The Spangler stress formula estimates the additional wall-bending stress due to vertical load, while the Iowa formula estimates pipe ovality ($Pipe_{ovality}$), which is the ratio of vertical deflection in a pipe cross section ($\Delta y$) to the pipe's outer diameter ($OD_{pipe}$) due to vertical load, as presented in figure 6. Figure 7 shows a stress distribution diagram for flexible pipes under a dead load.[19,20]

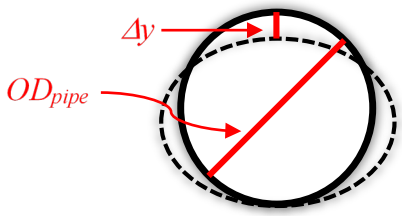




**Figure 6. Illustration. Ovality of a pipe cross section.**

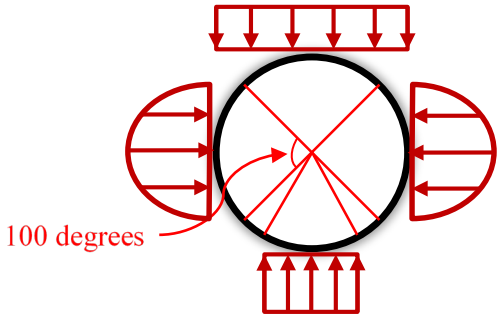




**Figure 7. Illustration. Stress distribution diagram for a flexible pipe under a dead load.**

Several agencies, including the U.S. Bureau of Reclamation, studied the Iowa formula, compared its estimates with field and laboratory tests, and generated what is referred to as the "Reclamation Equation."[22] The Reclamation Equation is a variation of the Iowa formula and incorporates modifications based on tests as well as studies on buried flexible pipes.

The Spangler stress formula and Iowa formula were examined in the CEPA report, and a modification to the Spangler stress formula was proposed.[20] The authors of the CEPA report concluded that they favor the use of Boussinesq-type expressions, which elastically combine the surface load transmitted to the buried pipeline, and Spangler-type calculations to compute induced pipe stresses. They extended the Spangler stress formula to include the beneficial effects of lateral soil restraint.[14] Table 2 provides a comparison of principle methods for evaluating vertical loading effects on buried pipelines.

**Table 2. Comparison of principle methods for evaluating vertical loading effects on buried pipelines.**

| Method | Strength | Limitation | Comments |
|---|---|---|---|
| Spangler stress formula | • Is easy to program.<br>• Includes pressure stiffening.<br>• Applies for full range of bedding angles. | Neglects soil restraint. | • Requires coefficients from the Boussinesq equation to estimate a load at the top of a pipe.<br>• Is considered conservative. |
| Iowa formula | • Is easy to program.<br>• Includes lateral soil restraint. | • Computes deflection, not stress.<br>• Neglects pressure stiffening.<br>• Needs to select soil parameter modulus of soil reaction ($E'$).<br>• Needs to select a lag factor. | Requires coefficients from the Boussinesq equation to estimate load at the top of a pipe. |

| Method | Strength | Limitation | Comments |
|---|---|---|---|
| | | • Is hardwired to 30-degree bedding angle. | |
| API RP 1102[21] | • Provides a detailed flow chart.<br>• Computes multiple stress components.<br>• Performs stress demand–capacity checks.<br>• Includes a check for fatigue. | • Is limited to auger bore construction.<br>• Is limited to cover depths ≥3 ft.<br>• Is hardwired to AASHTO H20 truck loads with tire pressures typically in excess of 80 psi. | • Is difficult to manually perform calculations.<br>• Requires PC-PISCES® or a technical toolbox. |
| Modified Spangler stress formula with soil restraint | • Is easy to program.<br>• Includes pressure stiffening.<br>• Includes lateral soil restraint. | • Needs to select soil parameter $E'$.<br>• Needs to select a lag factor. | • Requires coefficients from the Boussinesq equation to estimate a load at the top of a pipe.<br>• Removes some conservatism through the inclusion of soil restraint term. |

### 2.1.2 Methodology

The adopted methodology in this study is a hybrid step-by-step evaluation procedure provided in the ALA and the CEPA reports with special attention given to the method of determining the induced stresses on a buried pipe due to the application of a surface load.[19,20] The proposed modification utilizes the capabilities of 3D-Move Analysis software to realistically model the full pavement structure along with appropriate material properties.[10]

The procedure with the proposed modification is divided into the following four general checks:

- **Check 1**: Assess the factor of safety against the pipe circumferential stress failure ($FOS_{CSF}$).
- **Check 2**: Check $Pipe_{ovality}$ cross section.
- **Check 3**: Check the ring-buckling stress ($\sigma_{crb}$).
- **Check 4**: Check the wall-crushing stress ($\sigma_{wc}$).

The detailed steps involved with every check are described in the following subsections and implemented in the Superheavy Load Pavement Analysis PACKage software.[9]

***Check 1: Assess $FOS_{CSF}$***

To determine $FOS_{CSF}$, the equations in figure 8 through figure 14 are utilized. An $FOS_{CSF}$ greater than 1 indicates that the pipe integrity will not be affected due to internal pressure and external surface loads. Mitigation strategies should be invoked if $FOS_{CSF}$ is less than 1.

$$S_{hi} = \frac{P_{int}\left(OD_{pipe} - t_{pipe}\right)}{2 \times t_{pipe}}$$

**Figure 8. Equation. Circumferential stress due to internal pressure.**

Where:

$S_{hi}$ = pipe circumferential stress due to internal pressure.
$P_{int}$ = pipe internal pressure.
$t_{pipe}$ = thickness of the pipe wall.

$$R_W = 1 - 0.33\frac{h_w}{h_{cover}}$$

**Figure 9. Equation. Water buoyancy factor.**

Where:

$R_W$ = water buoyancy factor.
$h_w$ = height of water surface above the top of the pipe.
$h_{cover}$ = depth to the top of the pipe.

$$P_v = \gamma_{water} \times h_w + R_W \times \sigma_0$$

**Figure 10. Equation. Vertical stress due to dead load.**

Where:

$P_v$ = vertical stress due to dead load.
$\gamma_{water}$ = unit weight of water.
$\sigma_0$ = overburden pressure.

$$W_{vertical} = OD_{pipe}(P_v + P_p)$$

**Figure 11. Equation. Vertical load due to external dead and live loads.**

Where:

$W_{vertical}$ = vertical load due to external loads (dead and live loads).
$P_p$ = vertical stress due to live load.

$$\sigma_{bw} = \frac{3K_B\frac{W_{vertical}}{OD_{pipe}}\left(\frac{OD_{pipe}}{t_{pipe}}\right)^2}{1 + 3K_Z\frac{P_{int}}{E_{pipe}}\left(\frac{OD_{pipe}}{t_{pipe}}\right)^3 + 0.0915\frac{E'}{E_{pipe}}\left(\frac{OD_{pipe}}{t_{pipe}}\right)^3}$$

**Figure 12. Equation. Circumferential stress due to external dead and live loads.**

Where:

$\sigma_{bw}$ = circumferential stress due to external loads (dead and live loads).
$K_B$ = bending moment parameter.
$K_Z$ = deflection parameter.
$E_{pipe}$ = modulus of elasticity of the pipe.

$$\sigma_{bw\_total} = S_{hi} + \sigma_{bw}$$

**Figure 13. Equation. Total circumferential stress.**

Where $\sigma_{bw\_total}$ is the total circumferential stress due to internal pressure and external loads.

$$FOS_{CSF} = \frac{\sigma_{bw\_total}}{SMYS}$$

**Figure 14. Equation. Factor of safety against circumferential stress failure.**

Where *SMYS* is the specified minimum yield strength of pipe material.

It should be mentioned that $P_p$ in figure 11 is calculated using the Boussinesq equation. In this study, $P_p$ is determined using 3D-Move Analysis software so that the roles of pavement layers' stiffness properties, nonconventional SHL-vehicle tire and axle configurations, weight, and traveling speed are considered.(10) Alternatively, $P_p$ calculated in figure 15 is used to investigate $FOS_{CSF}$ of flexible buried utilities.

$$P_p = SAF_{Flexible}(\sigma_{zz\text{-}3D\text{-}Move})$$

**Figure 15. Equation. Modified vertical load due to external dead and live loads.**

Where:

$\sigma_{zz\text{-}3D\text{-}Move}$ = 3D-Move calculated vertical stress.
$SAF_{Flexible}$ = stress adjustment factor for a flexible pipe.

In this case, $\sigma_{zz\text{-}3D\text{-}Move}$ is calculated at the crown of the pipe. $SAF_{Flexible}$ accounts for the pipe flexibility and discontinuity in the medium due to the existence of buried utilities, as later discussed in chapter 3 of this report.

$K_B$ and $K_Z$ are Spangler stress formula parameters based on elasticity solutions for elastic-ring bending. They are functions of the bedding angle, as provided in table 3. A bedding angle of 30 degrees is typically used since it represents open-trench construction with relatively unconsolidated backfill. $E'$ can be assessed using the guidelines by Moser et. al.(11)

**Table 3. Spangler stress formula parameters.**

| Bedding Angle (Degrees) | $K_B$ | $K_Z$ |
|---|---|---|
| 0 | 0.297 | 0.110 |
| 30 | 0.235 | 0.108 |
| 60 | 0.189 | 0.103 |
| 90 | 0.157 | 0.096 |
| 120 | 0.138 | 0.089 |
| 150 | 0.128 | 0.085 |
| 180 | 0.125 | 0.083 |

### *Check 2: Check $Pipe_{ovality}$ Cross Section*

$Pipe_{ovality}$, which is the ratio of $\Delta y$ to $OD_{pipe}$, is calculated using the equations in figure 16 and figure 17. $Pipe_{ovality}$ greater than 5 percent indicates that the pipe integrity will be affected by the surface load applied; thus, mitigation strategies are required.

$$I_{pipe} = \frac{\left(t_{pipe}\right)^3}{12}$$

**Figure 16. Equation. Moment of inertia of the pipe wall cross section per inch of pipe.**

Where $I_{pipe}$ is the moment of inertia of the pipe wall cross section per inch of pipe.

$$Pipe_{ovality} = \frac{D_l K_b \left(P_v + P_p\right)}{\frac{\left(E_{pipe} I_{pipe}\right)}{\left(\frac{OD_{pipe}}{2}\right)^3} + 0.061 E'}$$

**Figure 17. Equation. $Pipe_{ovality}$ calculation.**

Where:

$D_l$ = deflection lag factor.
$K_b$ = bedding constant.

Note that $P_p$ in figure 17 is determined using the equation in figure 15 and $\sigma_{zz\text{-}3D\text{-}Move}$ at the crown of the pipe.

### *Check 3: Check $\sigma_{crb}$*

Figure 18 and figure 19 are used to calculate the allowable critical $\sigma_{crb}$. A combined induced $P_v$ and $P_p$ greater than $\sigma_{crb}$ indicates the need for mitigation strategies. As noted previously, 3D-Move Analysis software is used to determine $\sigma_{zz\text{-}3D\text{-}Move}$ to be used in the estimation of $P_p$ in figure 15.[10]

$$B' = \frac{1}{1 + 4e^{-0.065\frac{h_{cover}}{OD_{pipe}}}}$$

**Figure 18. Equation. Coefficient of elastic support.**

Where $B'$ is the coefficient of elastic support.

$$\sigma_{crb} = \frac{1}{FS_{req}}\sqrt{32 \times R_W \times B' \times E'\frac{\left(E_{pipe}I_{pipe}\right)}{OD_{pipe}^{\ 3}}}$$

**Figure 19. Equation. Allowable critical $\sigma_{crb}$.**

Where $FS_{req}$ is the required factor of safety for $\sigma_{crb}$, which is equal to 2.5 if the condition in figure 20 is satisfied. Otherwise, it is equal to 3.

$$\frac{h_{cover}}{OD_{pipe}} \geq 2$$

**Figure 20. Equation. Condition to determine $FS_{req}$.**

***Check 4: Check $\sigma_{wc}$***

$\sigma_{wc}$ calculated using the equations in figure 21 and figure 22 should be compared with the factor of safety against wall crushing stress ($FOS_{wc}$). Mitigation procedures should be invoked if $\sigma_{wc}$ is greater than $FOS_{wc}$ (figure 23).

$$T_{pw} = \frac{\left(P_v + P_p\right)\frac{OD_{pipe}}{12}}{2}$$

**Figure 21. Equation. Thrust in the pipe wall.**

Where $T_{pw}$ is the thrust in the pipe wall.

$$\sigma_{wc} = \frac{T_{pw}}{12\ t_{pipe}}$$

**Figure 22. Equation. $\sigma_{wc}$.**

$$FOS_{wc} = \frac{SMYS}{2}$$

**Figure 23. Equation. $FOS_{wc}$.**

Similar to checks 1–3, the induced $P_p$ is $\sigma_{zz\text{-}3D\text{-}Move}$ adjusted by $SAF_{Flexible}$ (figure 15).

## 2.2. PROCEDURE FOR RIGID UTILITIES

Buried utilities are mainly categorized as flexible or rigid based on the deflection of the utility. Flexible pipes should be able to withstand at least 2 percent deflection ratio (vertical deflection normalized with respect to the original size) without any significant structural distresses, while

rigid utilities do not meet this criterion. In this section, a literature review of rigid pipes and the AASHTO standard specifications methodology used in this study are presented.[16]

### 2.2.1 Background

Rigid utilities, based on the material type used in their construction, are mainly classified into three types: asbestos–cement pipe, clay pipe, and concrete utilities.[11,18] Due to hazardous risk associated with asbestos concrete, the use of asbestos–cement pipe has been limited. Clay pipe is manufactured from clay and shale. These pipes are resistant to corrosion and abrasion, but their strength is low. Concrete utilities, which are mostly reinforced, are manufactured and used in arch, pipe, and box (i.e., culvert) shapes. In this study, an analysis procedure to investigate the stability of a single-cell concrete box culvert subjected to an SHL-vehicle movement was considered. An illustration of a single-cell concrete box culvert, which is made up of four members (i.e., top slab, bottom slab, and two sidewalls) is depicted in figure 24.

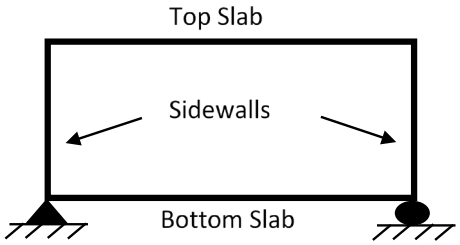



**Figure 24. Illustration. Single-cell concrete box culvert.**

After conducting an extensive literature review, it was decided to utilize the AASHTO standard specification to evaluate the vulnerability of a rigid utility subjected to an SHL-vehicle movement.[16] It is a common practice that consists of two main steps to design rigid buried utilities.[16] In the first step, the distribution of dead and live loads to the culvert loads is determined. The calculated distributed loads are used in the second step to design the rigid utility.

### 2.2.2 Methodology

Dead loads are the weight of earth fill (i.e., overburden) and self-weight of members. According to the AASHTO standard specification, the weight of the earth fill should be increased to consider the soil–structure interaction using the soil–structure interaction factor ($F_e$).[16] Figure 25 and figure 26 show equations to calculate $F_e$ for embankment or trench installation, respectively.

$$F_e = 1 + 0.2\frac{H_{culvert}}{B_{culvert}}$$

**Figure 25. Equation. $F_e$ for embankment installation.**

Where:

$H_{culvert}$ = embedment depth of the culvert from the surface.
$B_{culvert}$ = width of the culvert.

$$F_e = \frac{C_d B_{trench}^{\ 2}}{H_{culvert} B_{culvert}}$$

**Figure 26. Equation. $F_e$ for trench installation.**

Where:

$C_d$ = load coefficient for $F_e$ as specified in figure 27.
$B_{trench}$ = width of the trench.

The recommended values of the constant parameter as a function of soil type ($K\mu'$) defined in figure 27 can be found in table 4 for different soils.

$$C_d = \frac{1 - e^{-2K\mu'\left(\frac{H_{culvert}}{B_{trench}}\right)}}{2K\mu'}$$

**Figure 27. Equation. $C_d$ for trench installation.**

**Table 4. Recommended values of $K\mu'$.**

| Soil Type | $K\mu'$ |
|---|---|
| Cohesionless granular material | 0.1924 |
| Sand and gravel | 0.1650 |
| Saturated top soil | 0.1500 |
| Ordinary clay | 0.1300 |
| Saturated clay | 0.1100 |

To determine the live-load distribution on a rigid culvert, the AASHTO standard specification applies the tire loading of an HS20 truck at the surface of an unpaved SG soil (i.e., no CAB and AC layers).[16] Tire loading of 16,000 lb on a footprint of 10 by 20 inches was considered for an HS20 truck. The applied surface load is spread on top of the culvert with a rate of 1.00 or 1.15 as a function of soil type (figure 3). Subsequently, to consider the dynamic load allowance, the calculated load is increased by 33 percent for no cover depth and reduced to 0 percent for a depth of 8 ft.

The live-load distribution to the buried utilities due to SHL movement is determined using 3D-Move Analysis software.[10] $\sigma_{zz\text{-}3D\text{-}Move}$ on top of the rigid culvert is computed and adjusted by the stress adjustment factor for a rigid culvert ($SAF_{Rigid}$) to estimate the load distribution on top of the box culvert resulting from an SHL vehicle ($Load_{SHL}$) (figure 28). The determination of $SAF_{Rigid}$ is presented later in chapter 3.

$$Load_{SHL} = SAF_{Rigid}(\sigma_{zz\text{-}3D\text{-}Move}) l_{culvert} b$$

**Figure 28. Equation. Computation of live-load distribution on top of a concrete box culvert due to SHL-vehicle movement.**

Where:

$l_{culvert}$ = length of culvert opening.
$b$ = strip width (12 inches).

To investigate the internal integrity of a buried concrete box culvert (knowing the dead and live load distribution (figure 29)), calculating load-induced moment, shear, and axial forces in the members of the culvert (i.e., top slab, bottom slab, and sidewalls) is required. The slope-deflection method, which is a common structural analysis technique, was selected in this project since its solution scheme can be computationally solved.

Once the load-induced moment, shear, and axial forces are calculated for each of the concrete box culvert members, the stability of a rigid buried utility is investigated by analyzing the flexural strength, shear strength, and axial thrust ($P_u$) analysis in the concrete box culvert members (i.e., top slab, bottom slab, and sidewalls) in accordance with the AASHTO standard specification, which provides the specifications for the design of a concrete box culvert with known induced moment, shear, and axial forces.[16] Similarly, structural adequacy analysis is performed when the properties and characteristics of the concrete box culvert are known. These procedures are summarized in the following sections.

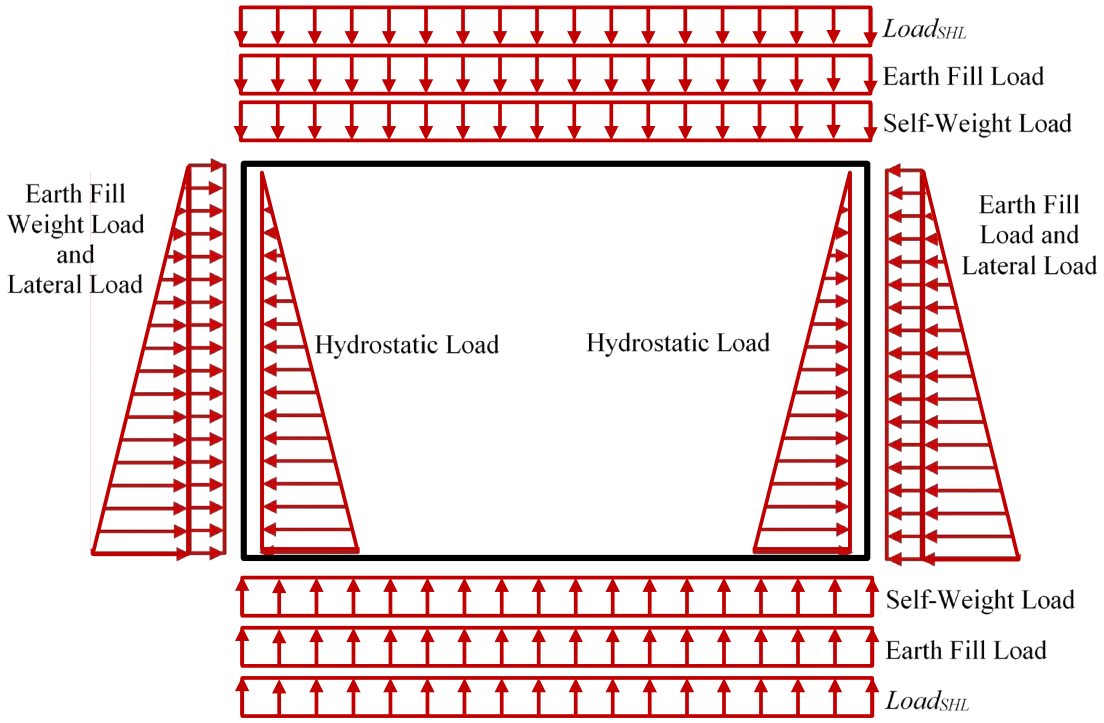




**Figure 29. Illustration. Applied load on a single-cell concrete box culvert.**

### *Flexural Strength Investigation*

The flexural strength of a concrete box culvert member is examined by comparing the factored flexural resistance ($\phi_f M_n$) and the maximum induced moment ($M_u$) at the cross section of the member. $\phi_f M_n$ is the product of strength reduction factor for flexure ($\phi_f$) and flexural resistance ($M_n$). The critical locations for flexural strength investigations are usually at the end and middle of the members. A value of $\phi_f M_n$ greater than $M_u$ indicates adequate flexural strength of the member. In this report, $\phi_f$ equals 0.9. The equations in figure 30 and figure 31 are used to calculate $M_n$.

$$d_e = t_{culvert} - Cover - D_{Reinforcement}$$

**Figure 30. Equation. Effective depth of a concrete box culvert member.**

Where, for a specific concrete box culvert member:

$d_e$ = effective depth.
$t_{culvert}$ = thickness of the culvert member.
$Cover$ = concrete cover on the reinforcements.
$D_{Reinforcement}$ = diameter of the longitudinal reinforcements.

$$M_n = A_s f_y \left( d_e - \frac{\frac{A_s f_y}{0.85 f'_c b}}{2} \right)$$

**Figure 31. Equation. Nominal $M_n$ of a concrete box culvert member.**

Where:

$A_s$ = available reinforcement area.
$f_y$ = yield strength of the reinforcement.
$f'_c$ = compressive strength of the concrete.

***Shear Strength Investigation***

In order to infer that a concrete box culvert member can resist the maximum induced shear ($V_u$), factored shear resistance ($\phi_s V_n$) of the member needs to be higher than $V_u$. $\phi_s V_n$ is the product of the strength reduction factor for shear ($\phi_s$) and shear resistance ($V_n$). In this report, $\phi_s$ equals 0.9. $V_n$ is calculated using the equations in figure 32 to figure 35.

$$d_v = \frac{M_n}{A_s f_y}$$

**Figure 32. Equation. Effective shear depth of a concrete box culvert member.**

Where $d_v$ is the effective shear depth.

$$V_c = 0.0316 \times 2 \sqrt{f'_c} (b d_v)$$

**Figure 33. Equation. Nominal shear strength of the concrete for culvert depth less than 2 ft.**

Where $V_c$ is the nominal shear strength of the concrete.

$$V_c = \left( 0.0676 \sqrt{f'_c} + 4.6 \frac{A_s V_u d_e}{b d_e |M_u|} \right) b d_e < 0.126 \sqrt{f'_c} (b d_e)$$

**Figure 34. Equation. $V_c$ for culvert depth greater than 2 ft.**

$$V_n = V_c + \frac{A_s f_y d_e}{S_{shear}}$$

**Figure 35. Equation. Nominal $V_n$ of a concrete box culvert member.**

Where $S_{shear}$ is the spacing of shear reinforcement.

### *$P_u$ Investigation*

The factored compressive axial resistance ($\phi_a P_n$) of the culvert members, which is determined using the equation in figure 36, needs to be higher than $P_u$ induced in the members. $\phi_a P_n$ is the product of strength reduction factor for compression ($\phi_a$) and compressive axial resistance ($P_n$). In this report, $\phi_a$ equals 0.7. It should be noted that the largest $P_u$ value is developed in the sidewalls.

$$P_n = 0.8\left(0.85 f_c^{'}\left(A_g - A_s\right) + f_y A_s\right)$$

**Figure 36. Equation. Nominal $P_n$ of a concrete box culvert member.**

Where $A_g$ is the gross area of a section.

# CHAPTER 3. STRESS ADJUSTMENT FACTOR FOR BURIED UTILITIES

In this chapter, the test results and observations from two experiments in a large-scale box (i.e., experiments No. 3 and No. 5) are presented. Experiment No. 3 is considered the control experiment and represents a full-scale pavement structure subjected to surface falling weight deflectometer (FWD) loads at different intensities without any cavities (i.e., no buried utilities). Experiment No. 5 models a similar pavement structure with two types of buried utilities installed in the SG subjected to the same surface FWD load intensities applied directly above the centerlines of the buried utilities. To determine $SAF_{Flexible}$ and $SAF_{Rigid}$, subsequent exercises compared induced vertical stresses computed using 3D-Move Analysis software to those measured in the experiments.[10]

## 3.1. DESCRIPTION OF EXPERIMENTS

Experiment No. 3 included FWD testing on the full pavement structure composed of 5 inches of AC, 6 inches of CAB, and 66 inches of SG. The following five FWD loads were applied at the pavement surface: 9,000; 12,000; 16,000; 21,000; and 27,000 lb. The instrumentation plans are presented in figure 37 to figure 40. Detailed discussions regarding the large-scale box experiments (e.g., construction procedure, instrumentation, and material properties) conducted as a part of this project are presented in Volume II: Appendix A.[2]

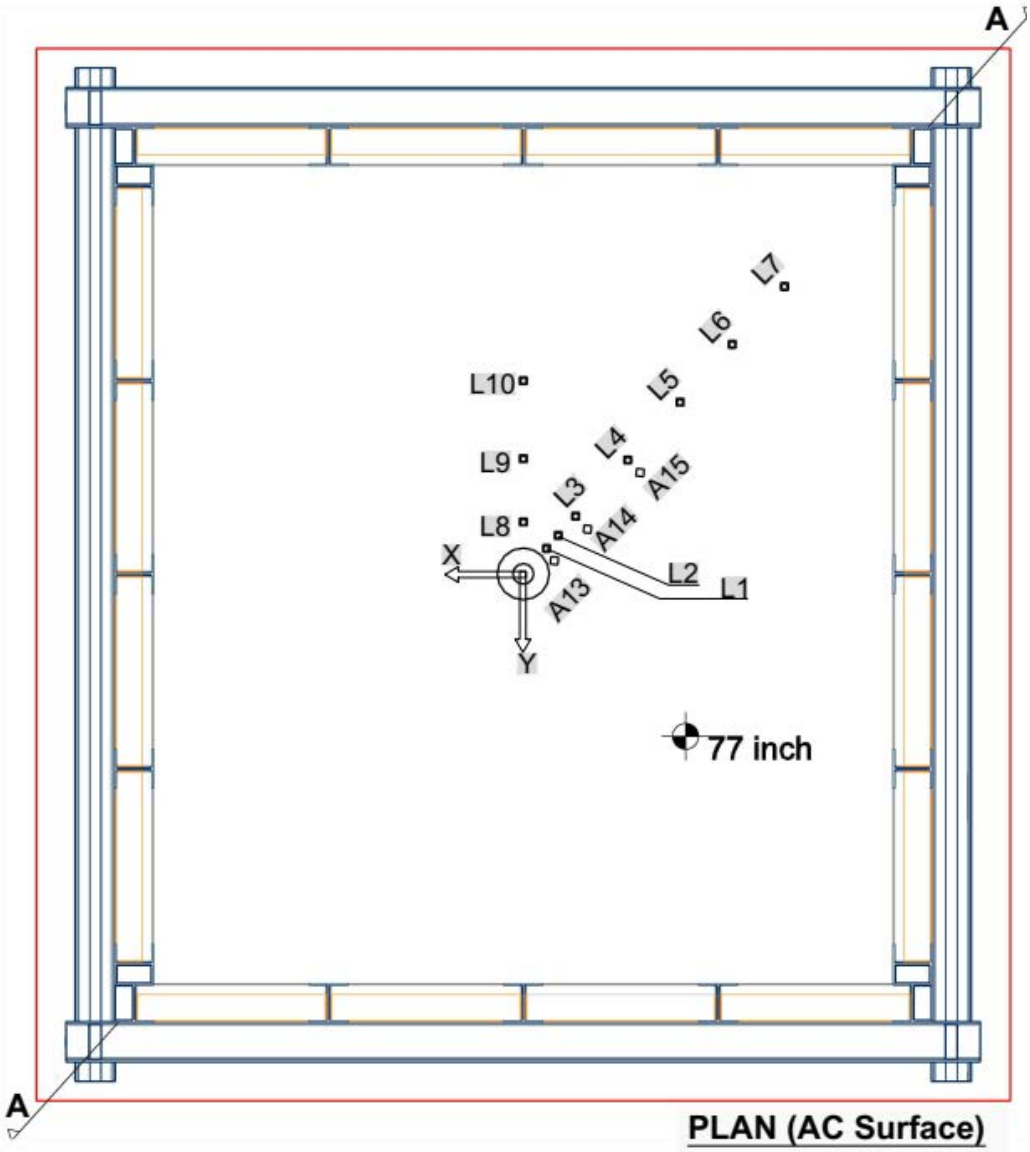



L = linear variable differential transformer (LVDT).
A = accelerometer.
Note: All dimensions are in inches.

**Figure 37. Illustration. Plan view for large-scale box instrumentation in experiment No. 3.**

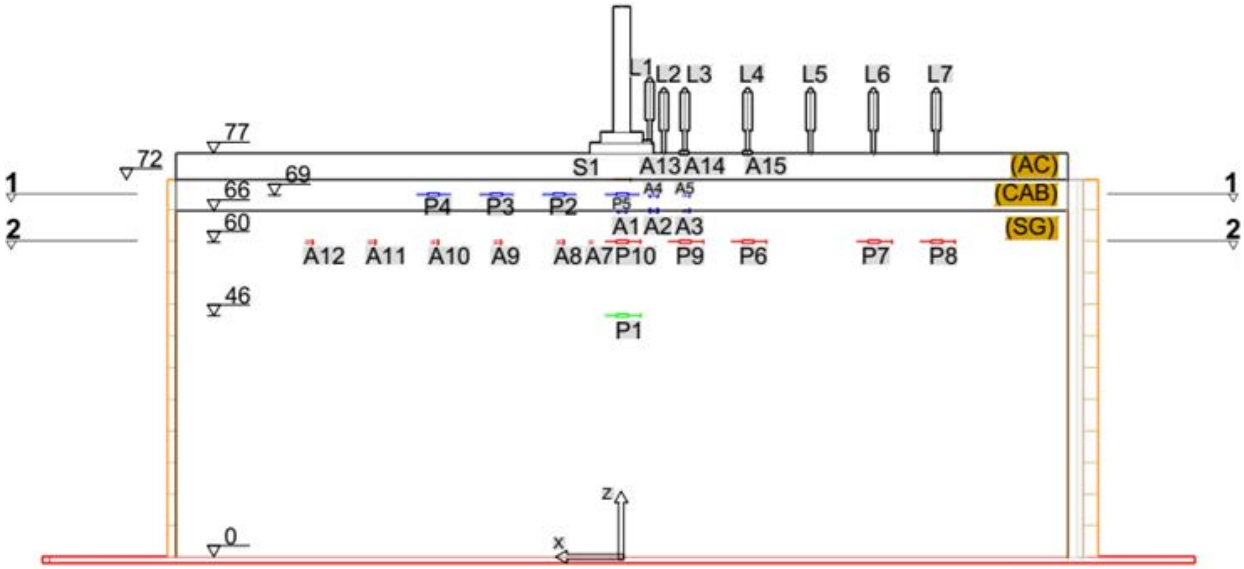


© 2018 UNR.
P = total earth pressure cell (TEPC).
Note: All dimensions are in inches.

**Figure 38. Illustration. Section A-A view for large-scale box instrumentation in experiment No. 3.**

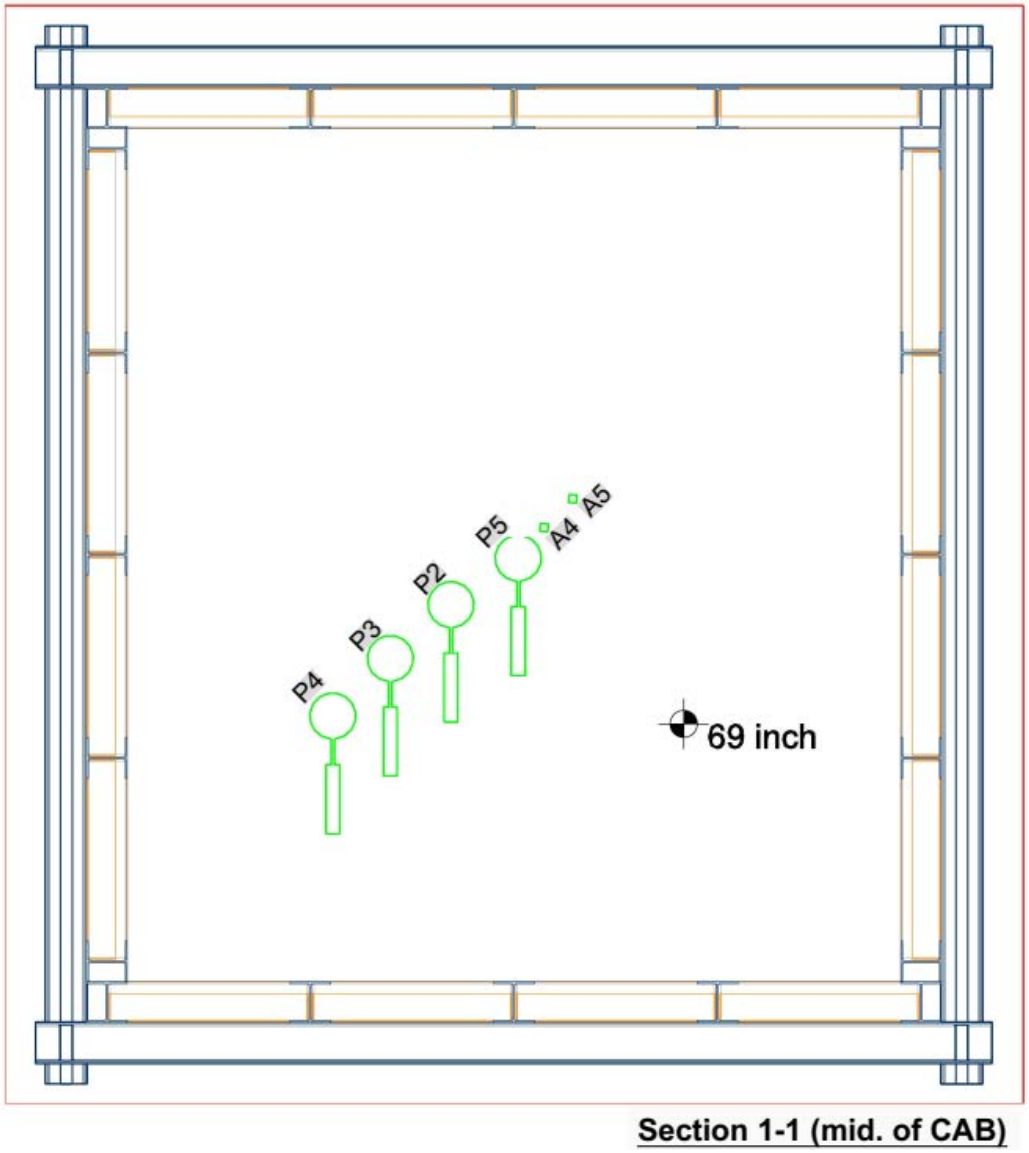



Note: All dimensions are in inches.

**Figure 39. Illustration. Section 1-1 view for large-scale box instrumentation in experiment No. 3.**

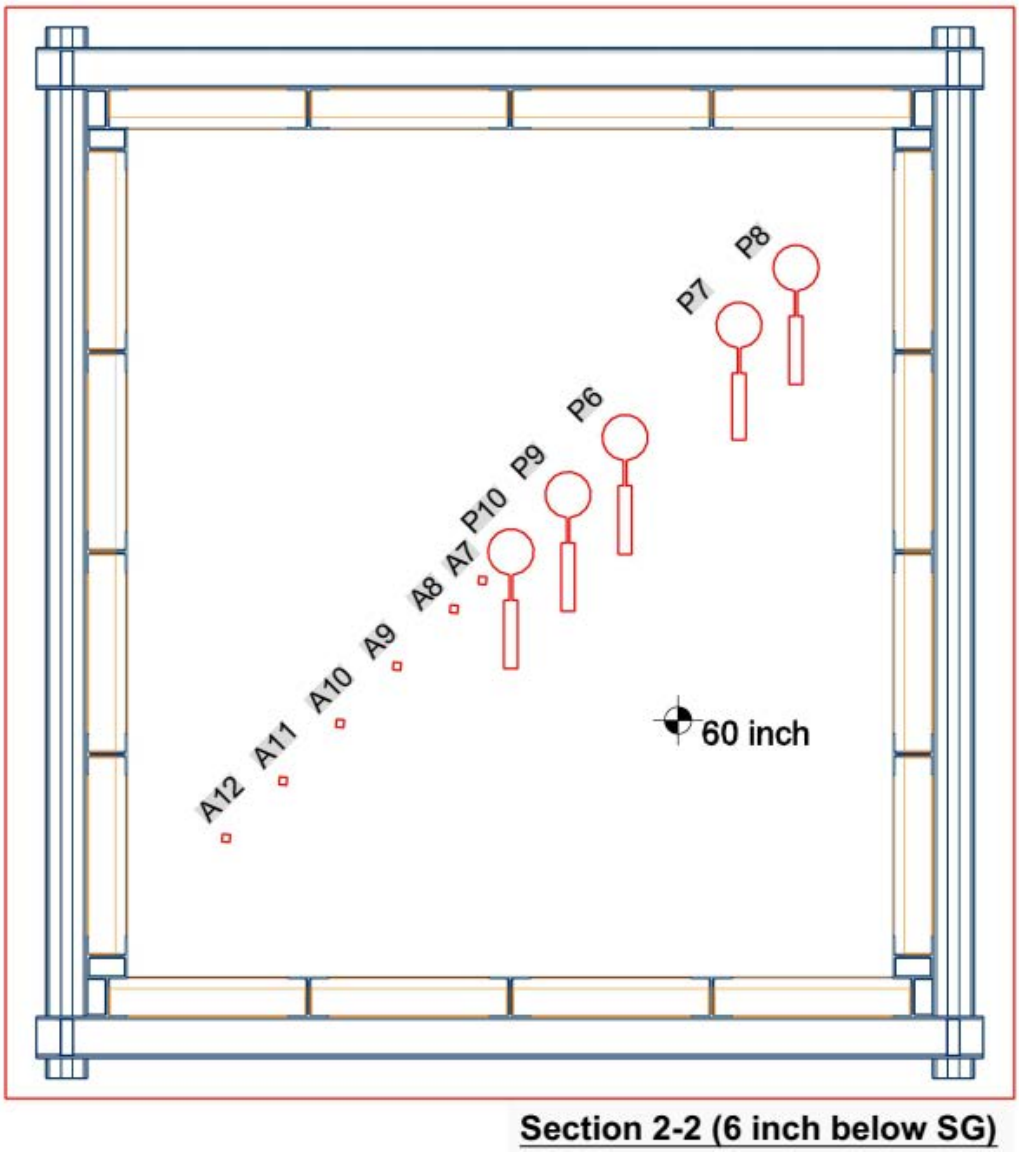



Note: All dimensions are in inches.

**Figure 40. Illustration. Section 2-2 view for large-scale box instrumentation in experiment No. 3.**

Experiment No. 5 was designed and executed to investigate the impact of SHL movement on buried utilities. The main objectives of the experiment were to: (1) study the effect of buried utilities on the distribution of induced internal stresses due to surface load, (2) verify the applicability of existing methods in assessing the increase in vertical stresses due to surface loads, and (3) determine adjustment factors $SAF_{Flexible}$ and $SAF_{Rigid}$. A full pavement structure, similar to that in the control experiment (experiment No. 3), was constructed for this purpose. Two types of buried utilities were installed in the SG: a 12-inch-diameter by 9-ft-long by 0.125-inch-thick steel pipe and a 12-inch-square cross section area by 9-ft-long by 1-inch-thick concrete box culvert. Various sensors were used to capture the responses of the pavement structure and the buried utilities. TEPCs were installed on top of and underneath the flexible pipe

and the concrete culvert to capture the induced pressure. LVDT sensors were installed inside both utilities to measure the vertical and the horizontal deformations. Foil rosette strain gauges were used on the steel pipe to measure the induced strain and calculate the corresponding stresses in the pipe wall.

The experiment was divided into three phases. In the first phase, FWD loads with different intensities ranging from 9,000 to 27,000 lb were applied at the surface (i.e., top of the AC layer) directly above the centerline of the flexible pipe. In the second phase, the same surface loads were directly applied above the centerline of the rigid culvert. In the third phase, the same surface loads were applied between the two buried structures. Figure 41 shows a schematic of the test setup and the three locations of surface load application. Volume II: Appendix A provides a complete description of the experiment, including the utility installation, the instrumentation plan, and the loading protocol.(2) The complete instrumentation plan is depicted in figure 42 through figure 49.

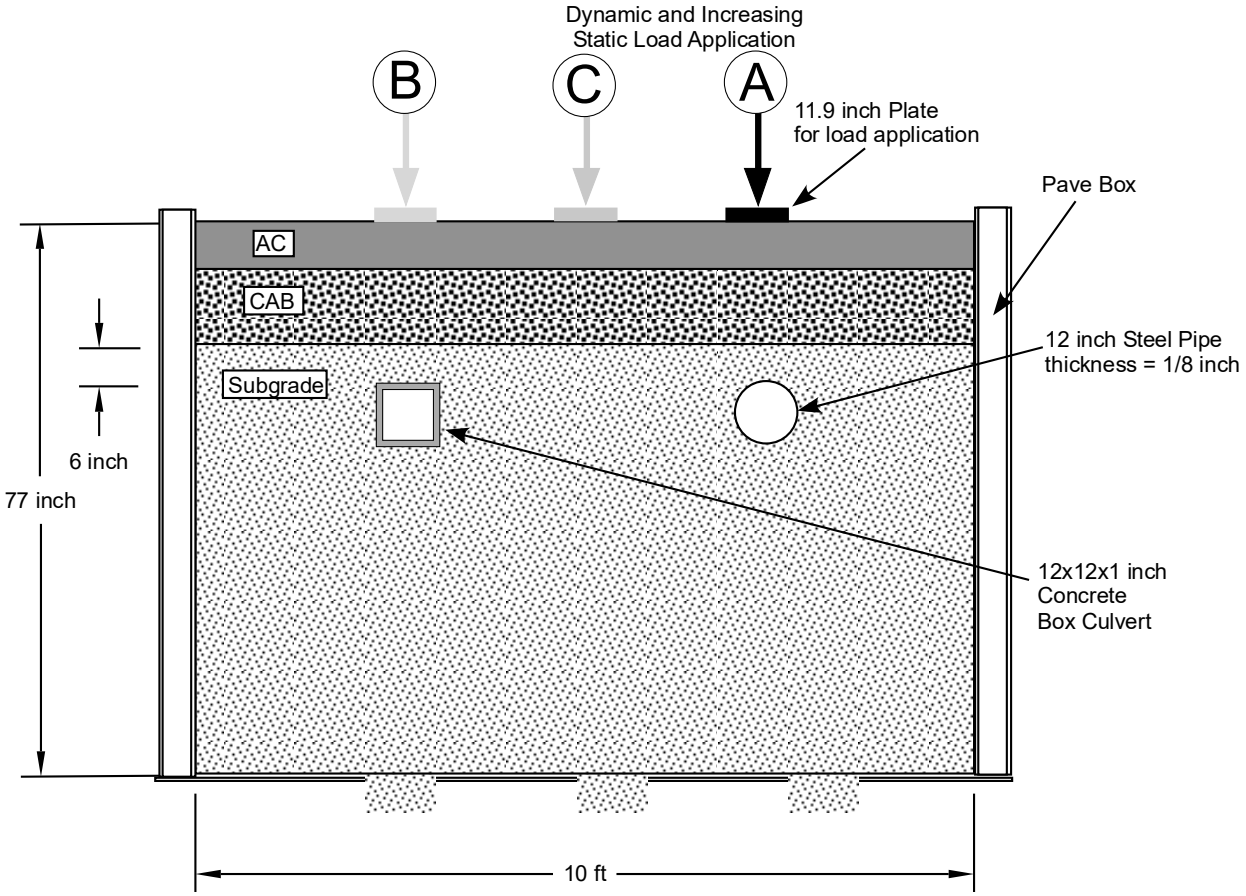



Note: A, B, and C denote locations A, B, and C.

**Figure 41. Illustration. Schematic of the test setup for experiment No. 5.**

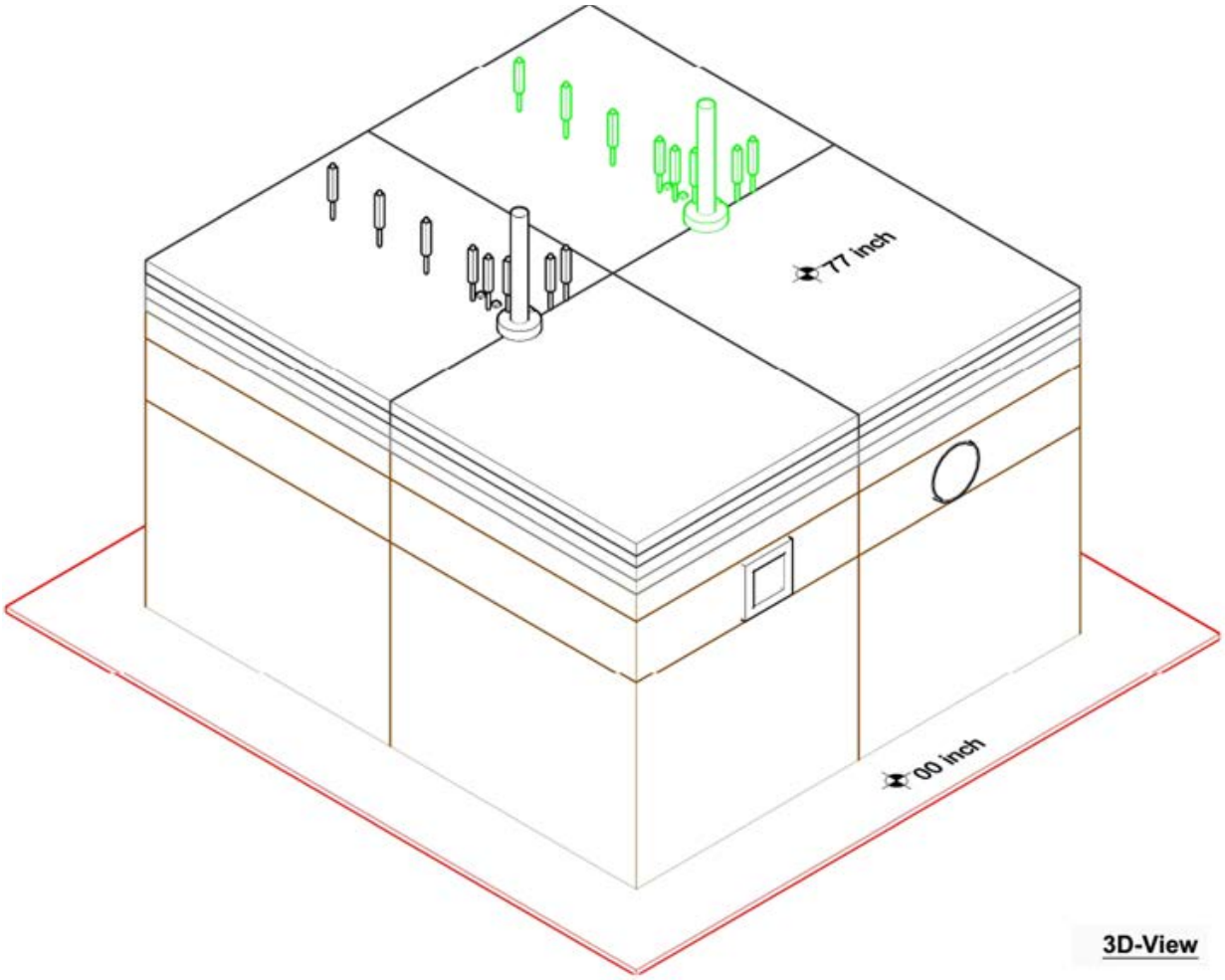



Note: All dimensions are in inches.

**Figure 42. Illustration. 3D view of large-scale box instrumentation in experiment No. 5 (depth of 77 inches).**

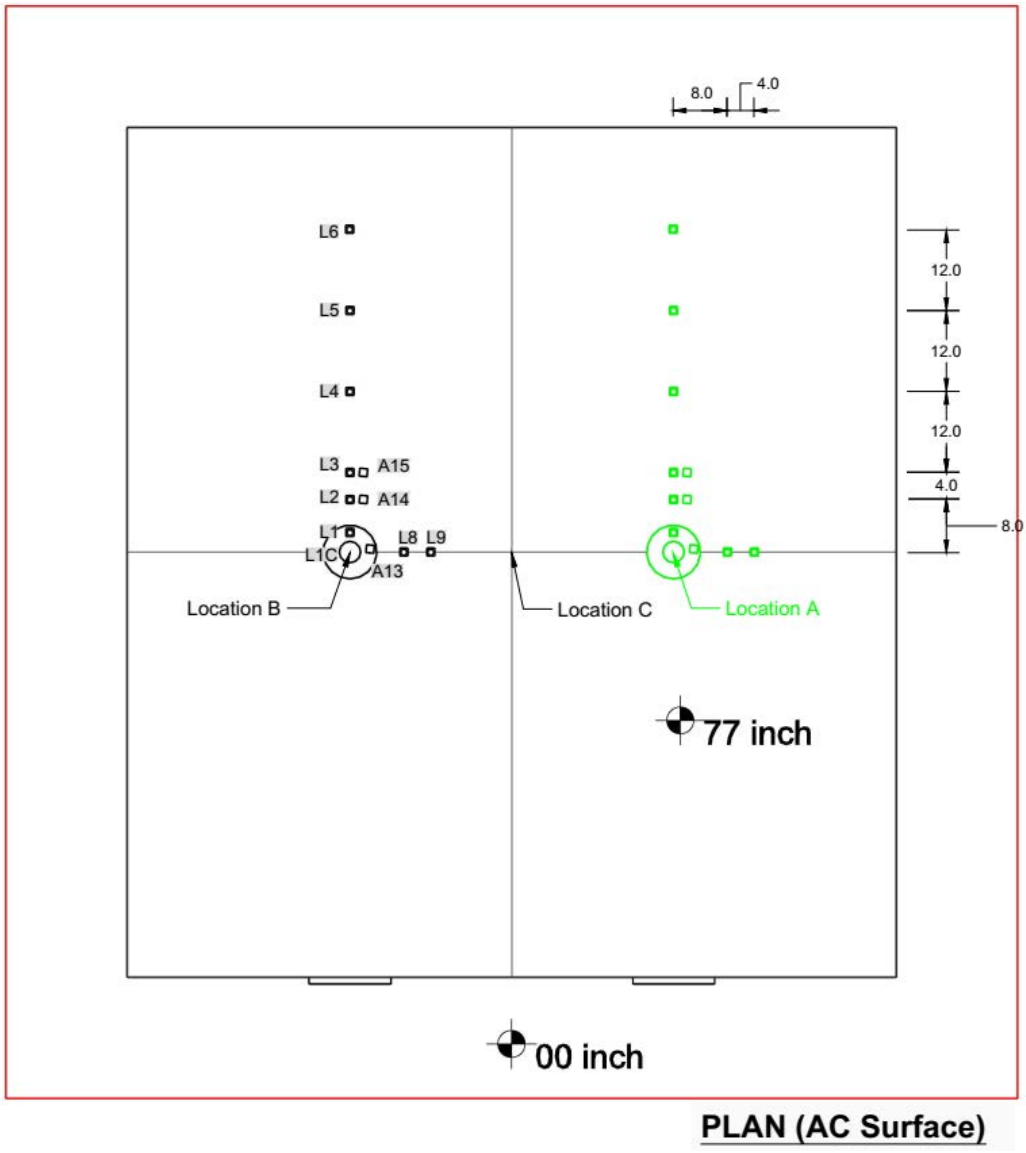



Note: All dimensions are in inches.

**Figure 43. Illustration. Plan view of large-scale box instrumentation in experiment No. 5 (depth of 77 inches).**

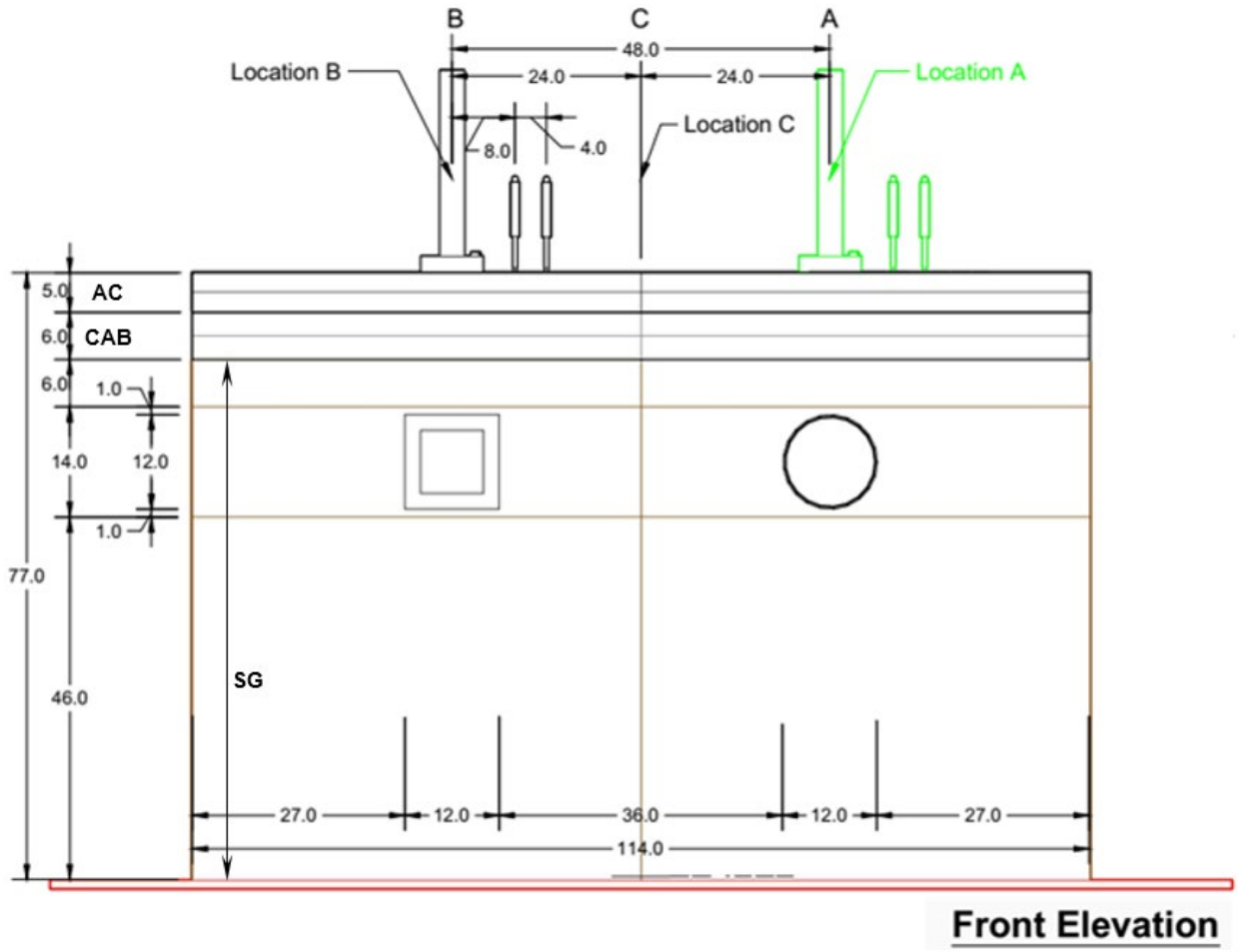



Note: A, B, and C denote locations A, B, and C. All dimensions are in inches.

**Figure 44. Illustration. Elevation of large-scale box instrumentation in experiment No. 5 (depth of 77 inches).**

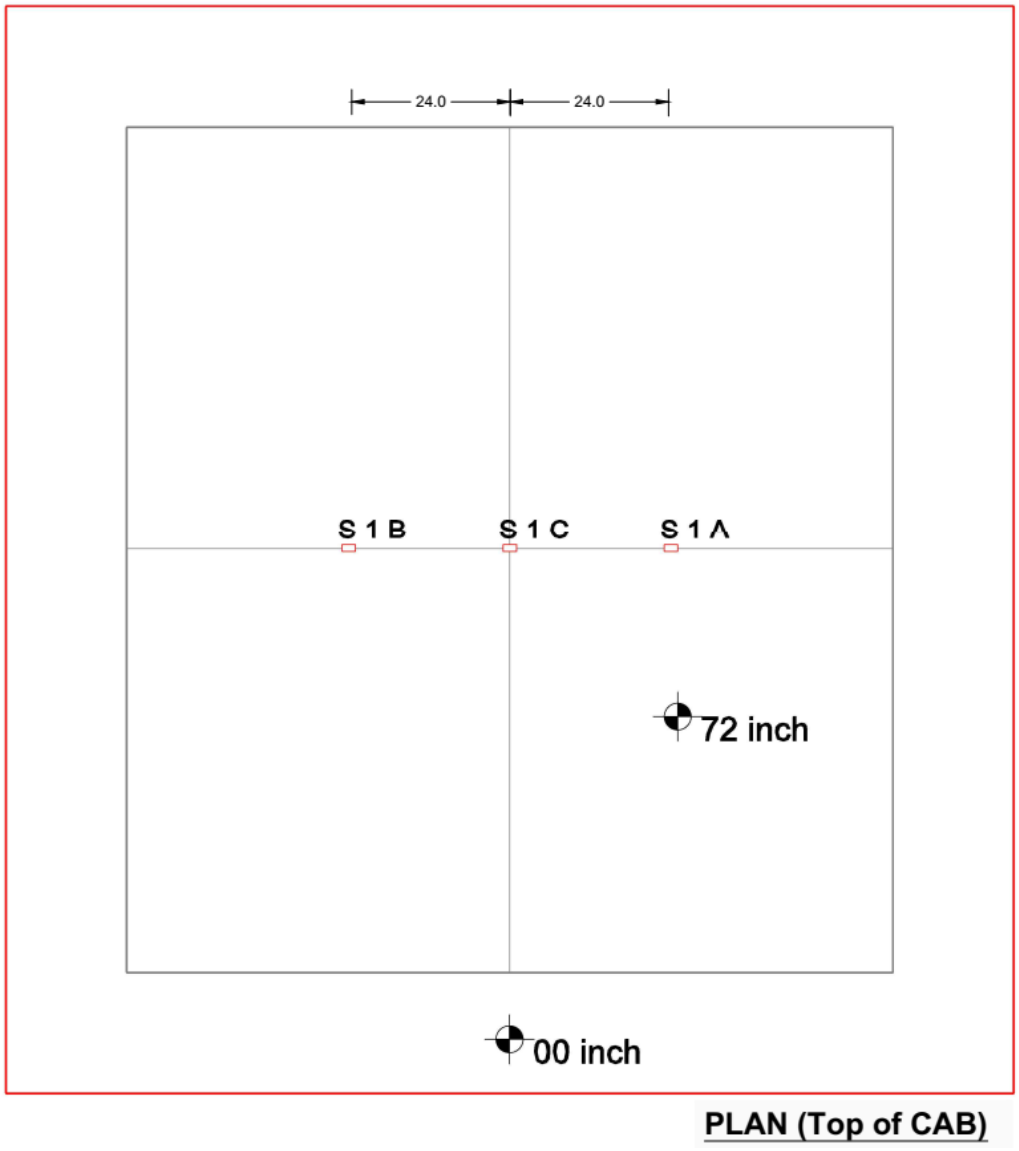



S = strain gauge.
Note: A, B, and C denote locations A, B, and C. All dimensions are in inches.

**Figure 45. Illustration. Plan view of large-scale box instrumentation in experiment No. 5 (depth of 72 inches).**

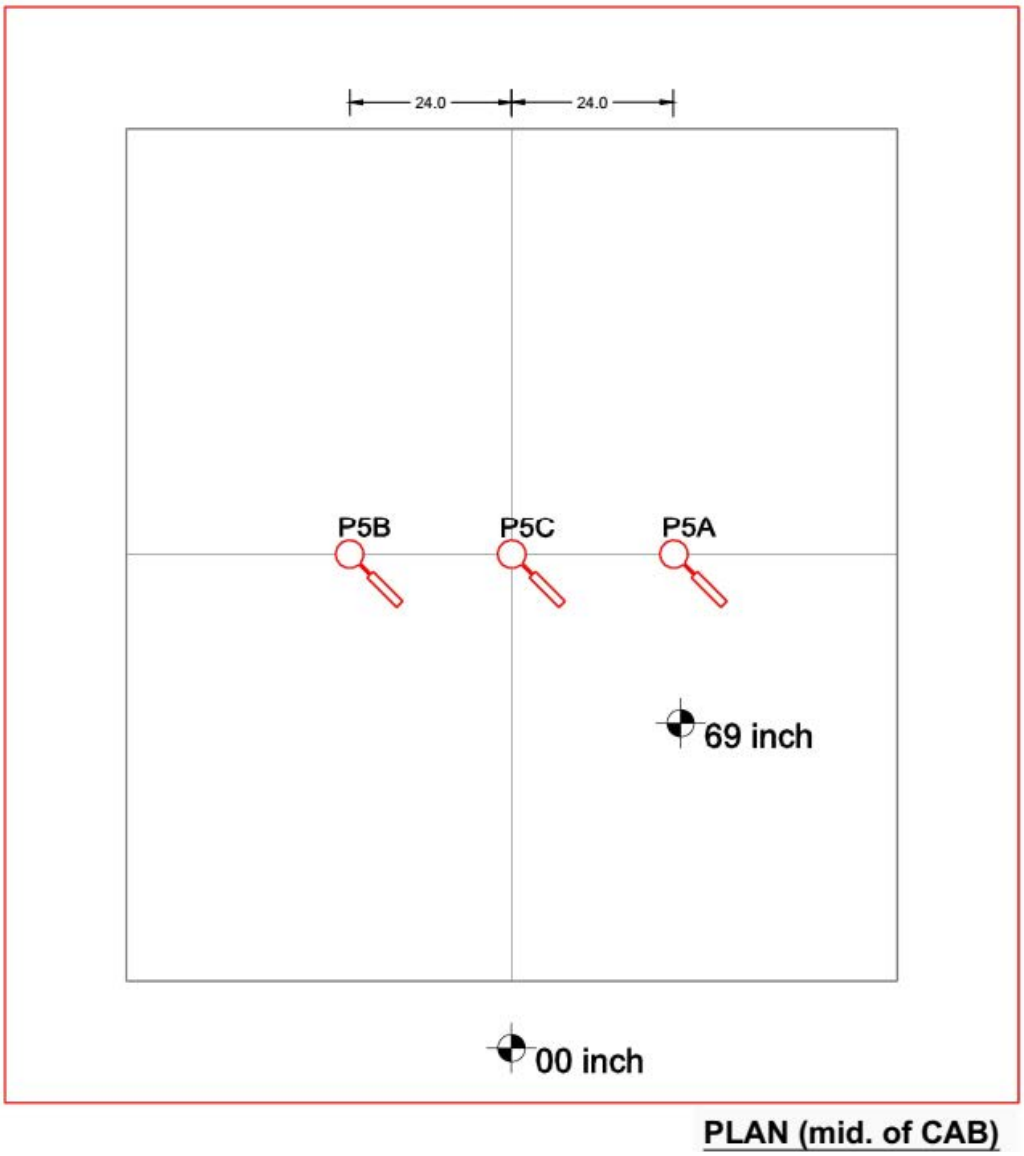



Note: A, B, and C denote locations A, B, and C. All dimensions are in inches.

**Figure 46. Illustration. Plan view of large-scale box instrumentation in experiment No. 5 (depth of 69 inches).**

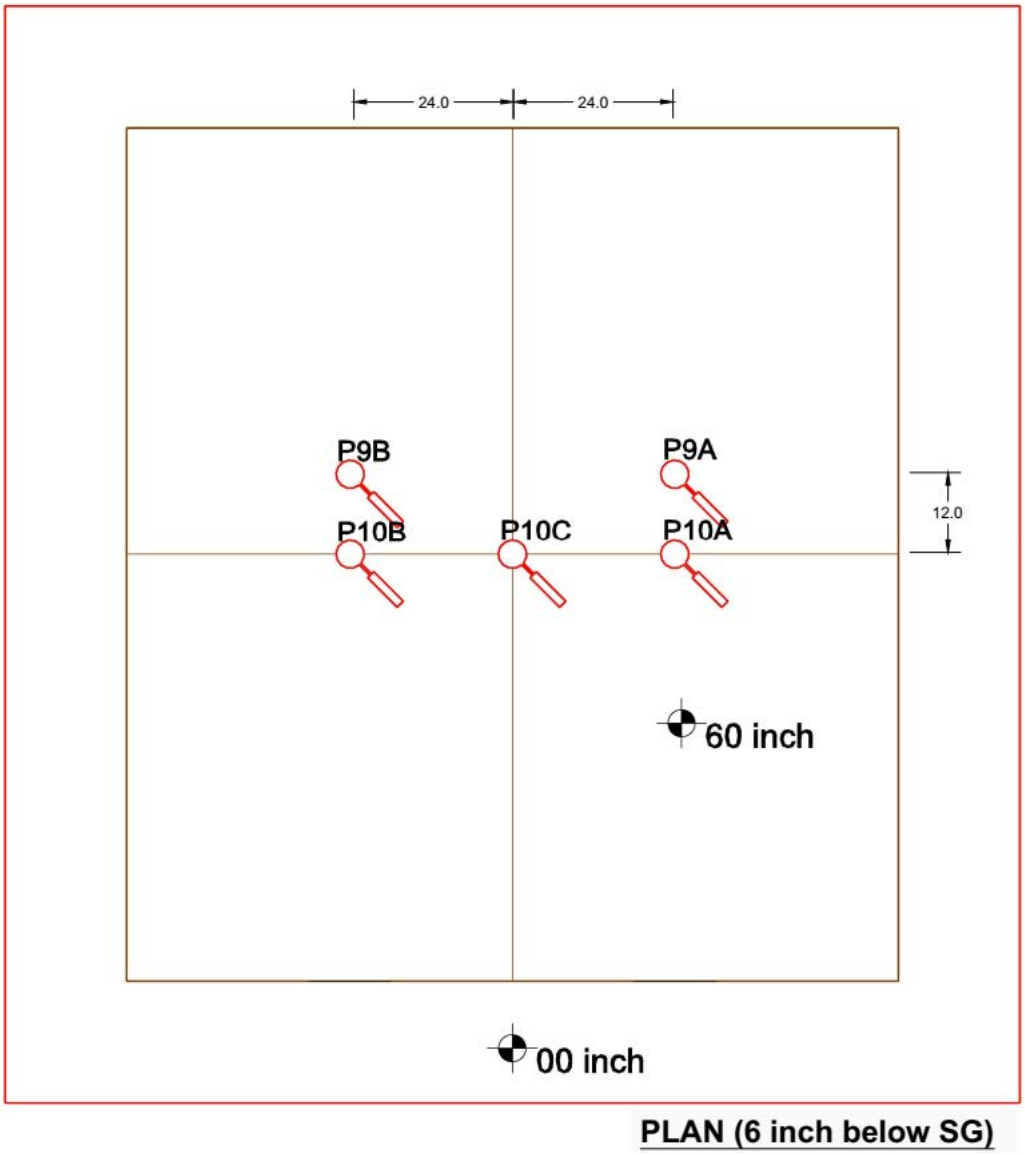



Note: A, B, and C denote locations A, B, and C. All dimensions are in inches.

**Figure 47. Illustration. Plan view of large-scale box instrumentation in experiment No. 5 (depth of 60 inches).**

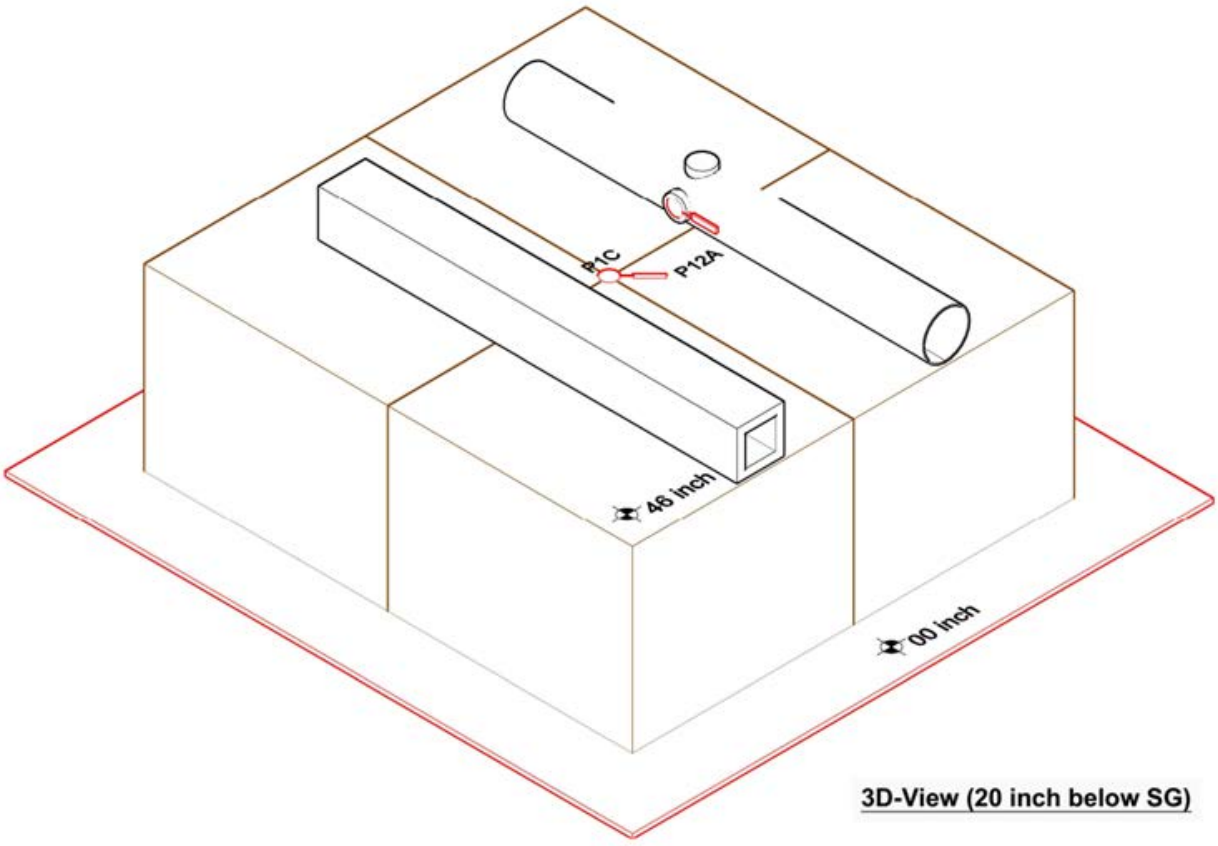



Note: A and C denote locations A and C. All dimensions are in inches.

**Figure 48. Illustration. 3D view of large-scale box instrumentation in experiment No. 5 (depth of 46 inches).**

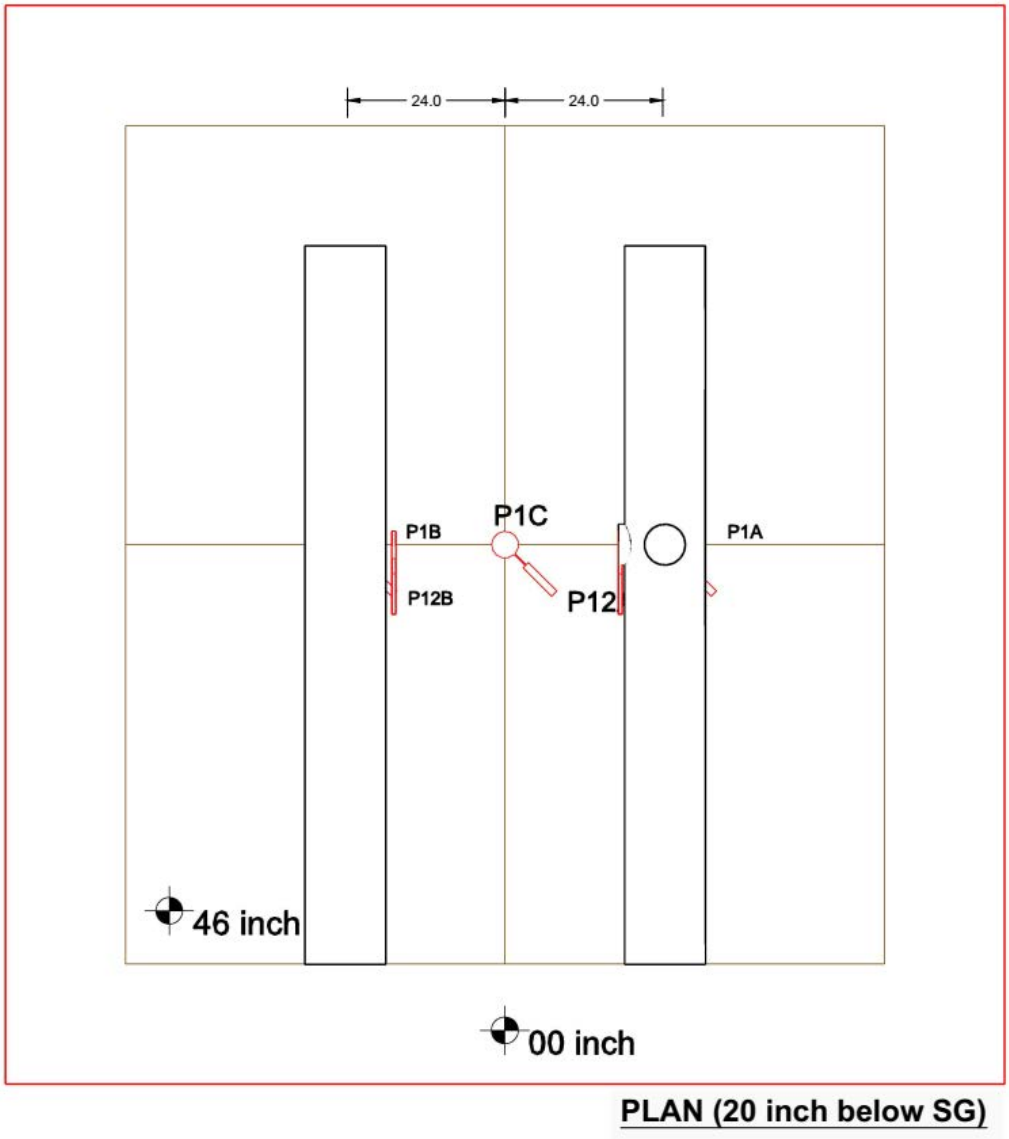



Note: A, B, and C denote locations A, B, and C. All dimensions are in inches.

**Figure 49. Illustration. Plan view of large-scale box instrumentation in experiment No. 5 (depth of 46 inches).**

In order to maximize the benefit from experiment No. 5, a suitable pipe diameter and wall thickness were selected so that the flexible pipe would act elastically at lower FWD load levels and yield or start to fail at higher FWD load levels. The procedure outlined in section 2.1 was used for the analysis without any adjustment to the stress calculation. In other words, 3D-Move Analysis software computed vertical stress at the location of the crown of the pipe without any adjustment.[(10)] An iterative process was carried out using different combinations of standard steel pipe diameters and wall thicknesses. After several trials, the 12-inch pipe (outer diameter) with 0.125-inch wall thickness was selected. According to the analysis, the pipe was expected to yield at the circumference (i.e., have circumferential stresses higher than yield stress) when the surface load exceeded 21,000 lb. The pipe was also expected to experience ovality higher than 5 percent at the same surface load level.

A criterion similar to the one outlined in section 2.2 was adopted for the culvert selection and design. The procedure used the same stresses assessed from 3D-Move Analysis software resulting from the FWD load levels (between 9,000 and 27,000 lb).[10] SAP2000®, a finite element program, was then used to determine the induced moment, shear, and axial forces on the culvert members.[23] Readily available culvert sections were checked first. It was concluded that these sections were too thick and would not experience any significant failure even at higher load levels. Consequently, it was decided to build a section with a wall thickness that could potentially endure failure at higher load levels. A square cross section with outer dimensions of 12 by 12 inches and 1 inch of wall thickness was selected since it was easier to construct and consistent with the steel pipe size. The SAP2000® analysis of the cross section showed that the wall thickness should allow the box culvert to experience some damage at higher load levels. A concrete strength of 4,000 psi was assumed for the analysis.

## 3.2. EXPERIMENTAL RESULTS AND OBSERVATIONS IN EXPERIMENT NO. 3

In order to determine stress adjustment factors, the measured stresses at the location of TEPCs in experiment No. 5 need to be compared against the respective calculated stresses from 3D-Move Analysis software.[10] The backcalculated moduli for the various layers from experiment No. 3 were used in 3D-Move Analysis software simulations since this experiment was intended to be a control experiment representing pavement structure without any buried utility.

Figure 50 presents the maximum pavement surface vertical deflections from LVDT measurements (averaged from five cycles) at each of the applied load levels in experiment No. 3. The surface deflection basins at different load levels were employed in the backcalculation analysis using the program BAKFAA.[24] Repeated attempts at the backcalculation process with many controls on the variability of the elastic modulus revealed that the SG layer should be subdivided to two sublayers using the Depth to an Apparent Rigid Layer method.[25]

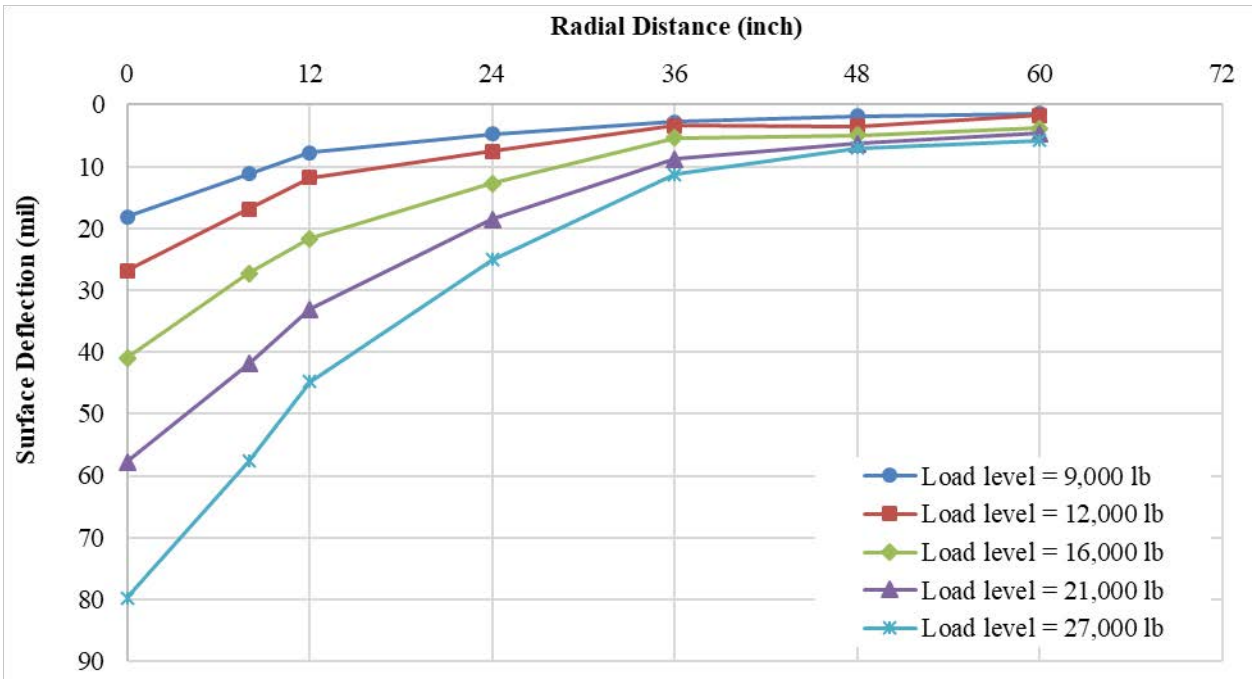




**Figure 50. Graph. Measured deflection basin in experiment No. 3.**

Figure 51 depicts the comparison between the vertical stresses at the location of TEPCs (P1, P3, P5, P6, P9, and P10 (figure 38)) in experiment No. 3 and those calculated by 3D-Move Analysis software using associated backcalculated moduli.[10] These observations revealed the capability of 3D-Move Analysis software to estimate the load-induced stresses when the pavement layers extend laterally to infinity without any discontinuities (i.e., no buried utilities).

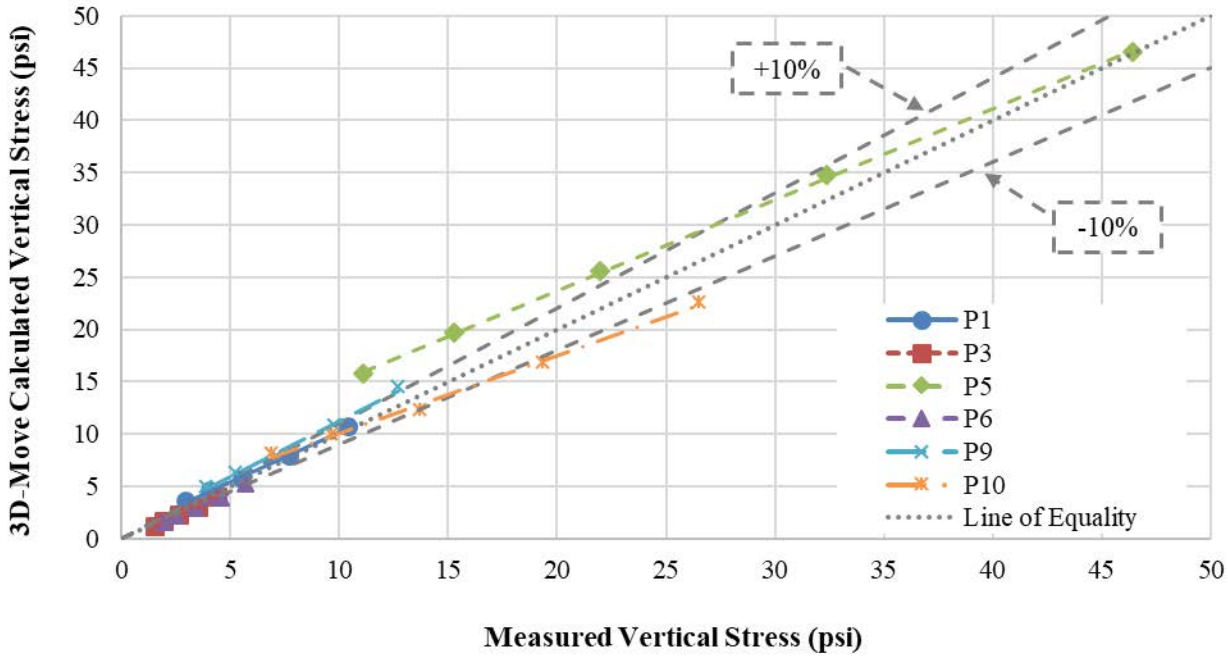



P = TEPC.

**Figure 51. Graph. Comparison between 3D-Move Analysis software-computed versus measured vertical stresses in experiment No. 3.**

## 3.3. EXPERIMENTAL RESULTS AND OBSERVATIONS FOR FLEXIBLE PIPE

In this section, the test results and observations obtained from experiment No. 5 when the surface loads were on the centerline of flexible pipe are presented. One important observation made after the conclusion of experiment No. 5 was that the pipe never experienced any failure at any surface load level. Although the pipe was expected to yield and experience excessive ovality when the surface load reached 21,000 lb, the pipe integrity remained undamaged, even at a surface load of 27,000 lb. This observation pointed to the fact that the pipe experienced much lower stresses than the computed stresses with 3D-Move Analysis software (without any adjustment for vertical stresses).

### 3.3.1 Comparison of Pressure Cells

TEPCs were used to capture the changes in stresses due to surface loads. In experiment No. 5, TEPCs were installed at the crown (top) and the invert (bottom) of the pipe using a special mold to attach them to the pipe's surface. Data obtained from these TEPCs were compared to the data obtained from TEPCs from experiment No. 3 installed at the same locations and depths. Figure 52 shows the measured vertical stresses by the TEPC installed at the crown of the pipe in experiment No. 5 (P10A) when the load was applied at the centerline of the pipe (i.e., location A). As shown in figure 52, the vertical stresses experienced by the flexible pipe were much lower than those stresses transferred in a continuum medium measured by P10 in experiment No. 3. Thus, it can be concluded that presence of flexible pipes affects the vertical stress distribution.

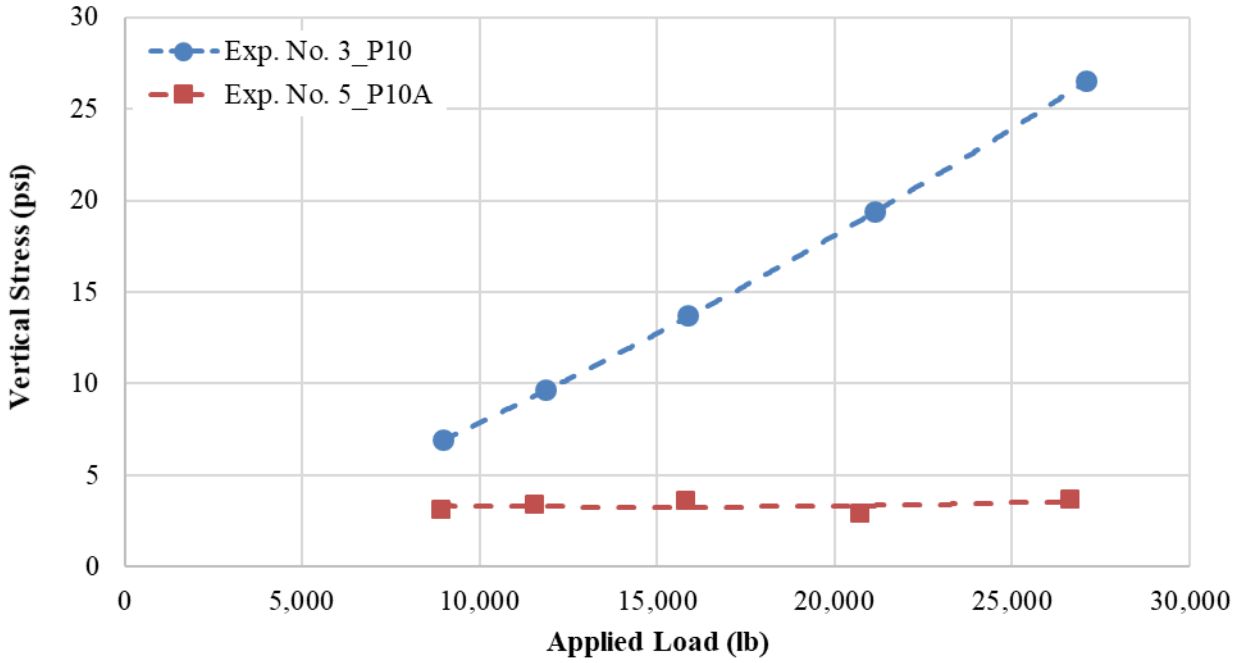




**Figure 52. Graph. Measured vertical stresses by P10 in experiment No. 3 and P10A in experiment No. 5.**

Figure 53 shows the vertical stresses measured by TEPC installed at the invert of the pipe in experiment No. 5 (P1A) and the TEPC installed at the same depth and location in experiment No. 3 (P1) as a function of the applied surface load. As shown in the figure, there are no significant changes in the stresses due to the presence of the flexible pipe. One possible explanation for this observation is that the presence of the flexible pipe redistributed the stresses and affected the stress flow near and around the pipe. Unfortunately, the TEPC installed on the side of the pipe to measure horizontal stresses, as well as the strain gauges installed on the pipe walls, malfunctioned at the early stages of the experiment and did not provide any data to allow further investigation.

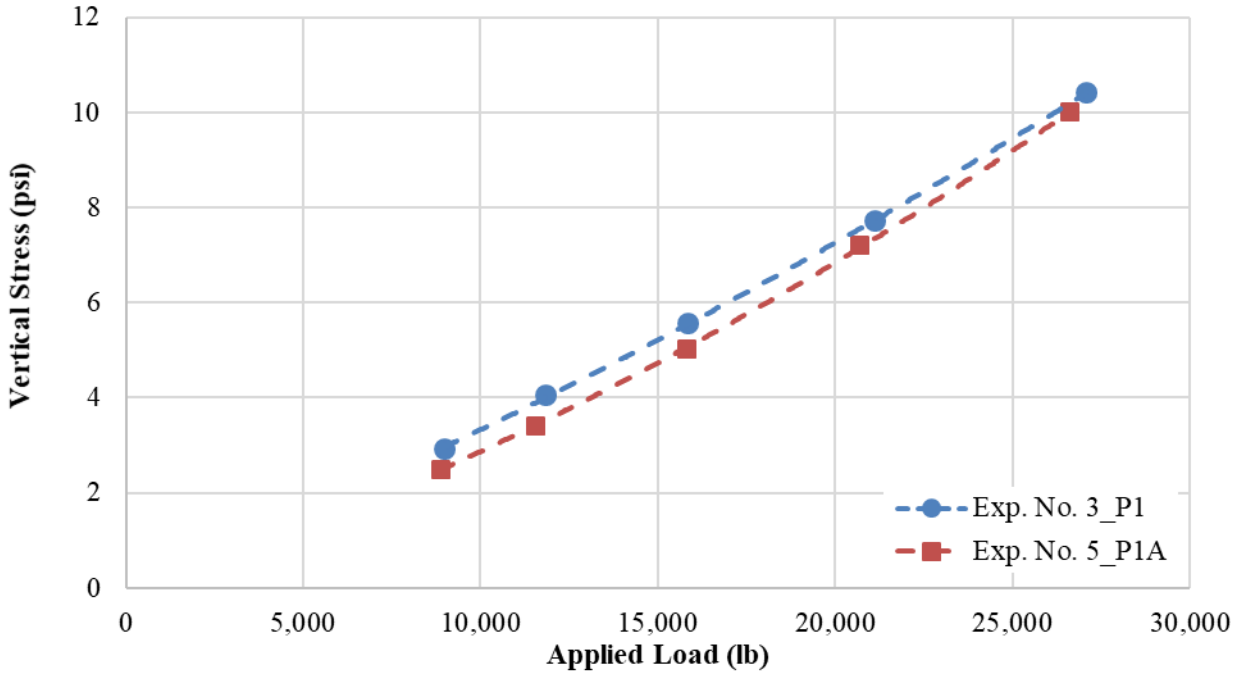




**Figure 53. Graph. Measured vertical stresses by P1 in experiment No. 3 and P1A in experiment No. 5.**

Data from the TEPCs were also compared to the elastic solution calculated using the Boussinesq equation, which is commonly used in current practices to estimate the increase in vertical stresses on buried pipes due to surface loads.[19,20] The Boussinesq equation requires an estimate of the depth of soil cover above the pipe, ignoring any soil layering and the effect of their stiffness in redistributing the stresses. This practice is usually acceptable if the soil layers have comparable stiffness. However, in pavement structures, the AC and CAB layers have significantly higher stiffnesses than the SG. Thus, two types of calculations were carried out. The first one was conducted by ignoring the layering and assuming total cover depth equal to 17 inches (5 inches for AC, 6 inches for CAB, and 6 inches for SG). The second calculation used the backcalculated moduli of the pavement layers from experiment No. 3 (i.e., control experiment) along with the 3D-Move Analysis software.[10] Figure 54 compares the measured stresses at the crown of the pipe against computed stresses using 3D-Move Analysis software and the Boussinesq equation. None of the methods were able to accurately estimate the vertical stresses at the crown of the pipe.

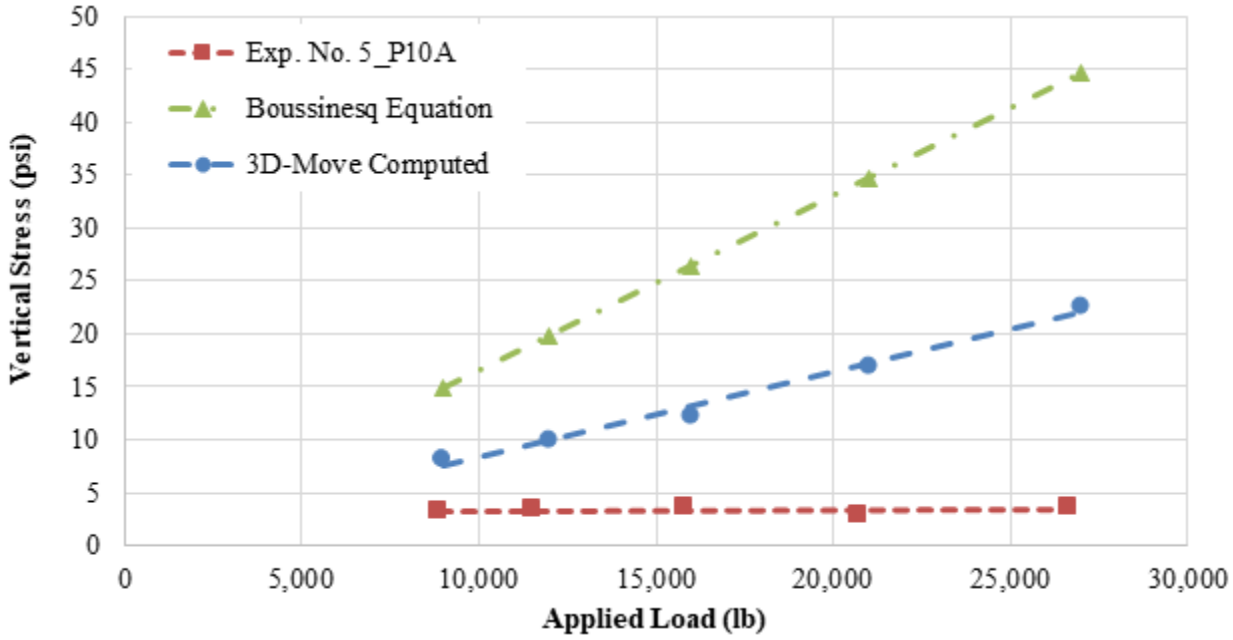




**Figure 54. Graph. Comparison between measured and computed stresses at the crown of the pipe.**

### 3.3.2 Ovality Check

Two LVDTs perpendicular to one another were installed inside the pipe to capture the horizontal and vertical deformations (i.e., change in pipe diameter). Data from the vertical LVDT were used to calculate $Pipe_{ovality}$. $Pipe_{ovality}$, as defined in section 2.1 and presented in figure 17, is the ratio of $\Delta y$ to $OD_{pipe}$. Figure 55 shows the vertical and horizontal deflections in a pipe cross section for all load levels. The negative signs on the y-axis indicate that the deflection was inward, meaning that the pipe diameter in the vertical deflection decreased with load. As presented in the figure, the maximum deflection was about 0.041 inch at a surface load of 26,631 lb. This translates to a $Pipe_{ovality}$ of 0.34 percent. Using the procedure outlined in section 2.2, the vertical stress at the crown of the pipe was backcalculated to cause such ovality. The calculated stress of 1.3 psi shows that it was very close to the measured stress and not to any of the calculated stresses. Thus, more confidence was gained in the measured values.

Although a deflection of 0.041 inch is very small and does not indicate any yielding in the pipe, a comparison was made between the vertical and horizontal LVDTs to see if the pipe deformed elastically. As shown in figure 55, the response was the inverse, yielding to the realization that the pipe remained elastic during the load application.

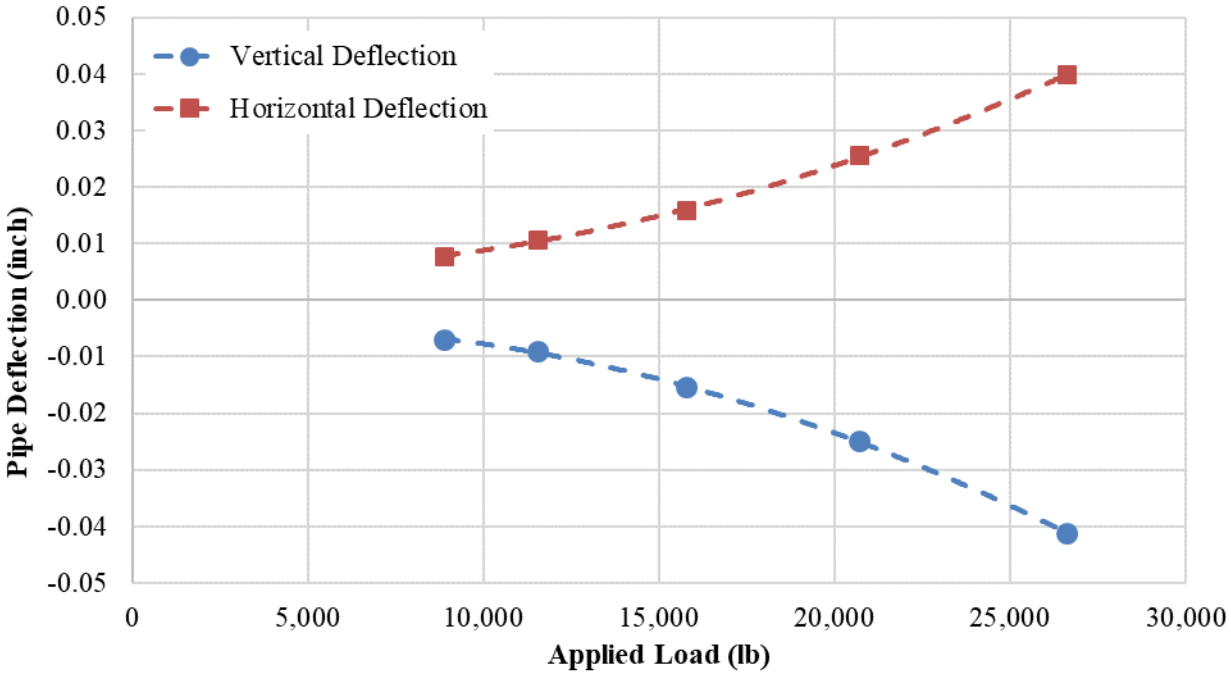



**Figure 55. Graph. Vertical and horizontal deformations in the pipe cross section.**

### 3.3.3 Other Observations

Another observation was made when analyzing the stress response obtained from the TEPC installed at the crown of the steel pipe (P10A). As the surface load increased, the TEPC reported a stress response that was out of sync with surface loading and unloading. Figure 56 and figure 57 present the TEPC data recorded as a function of time in seconds at 9,000 and 27,000 lb, respectively. As shown in figure 56, TEPC readings were positive, which indicates an increase in pressure due to loading. However, figure 57 shows TEPC readings that were negative. Since TEPC measures the change in stresses from the overburden static condition, these readings indicate stresses lower than the overburden pressure. This behavior may be attributed to either soil arching or a case where AC and CAB layers recovered from the dynamic loads faster than the steel pipe recovered. It should be noted that this behavior was not sudden. It started to develop at a surface load of 16,000 lb and was pronounced when the load increased to 27,000 lb.

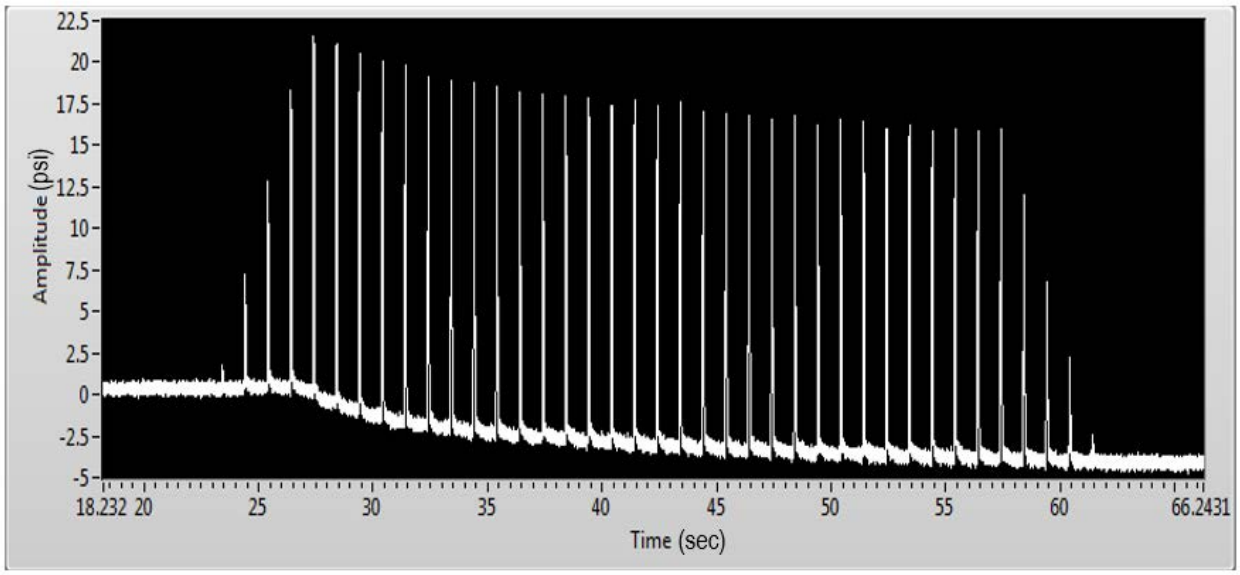




**Figure 56. Graph. TEPC data at the crown of the steel pipe (P10A) at 9,000-lb surface load.**

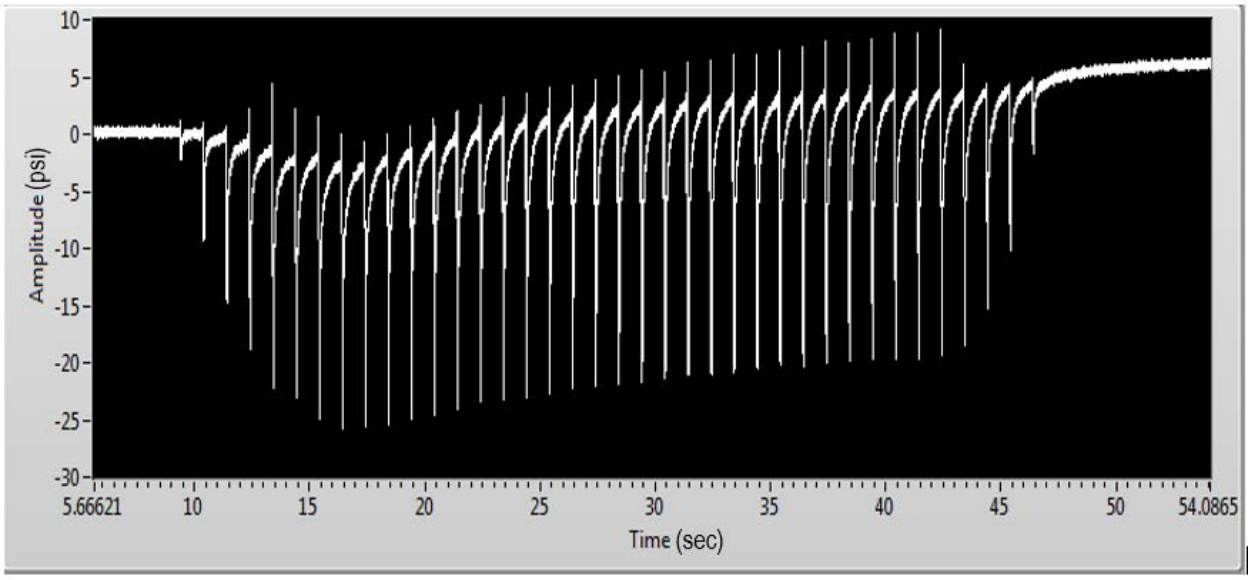




**Figure 57. Graph. TEPC data at the crown of the steel pipe (P10A) at 27,000-lb surface load.**

Furthermore, on examining one cycle of the stress response recorded by P10A corresponding to one cycle of surface load of 27,000 lb, an interesting behavior was observed. As shown in figure 58, the TEPC reported lower vertical stress as the surface FWD-type pulse load started to gradually increase. However, as the load continued to increase in magnitude, the vertical stress reversed course and started to recover. Once the pulse load reached its peak, the vertical stress started to decrease again until the pulse load was removed. Once the load was removed, the vertical stress started to slowly recover. This behavior is attributed to the soil–structure (i.e., pipe) interaction, which requires further investigation that is outside the scope of this study.

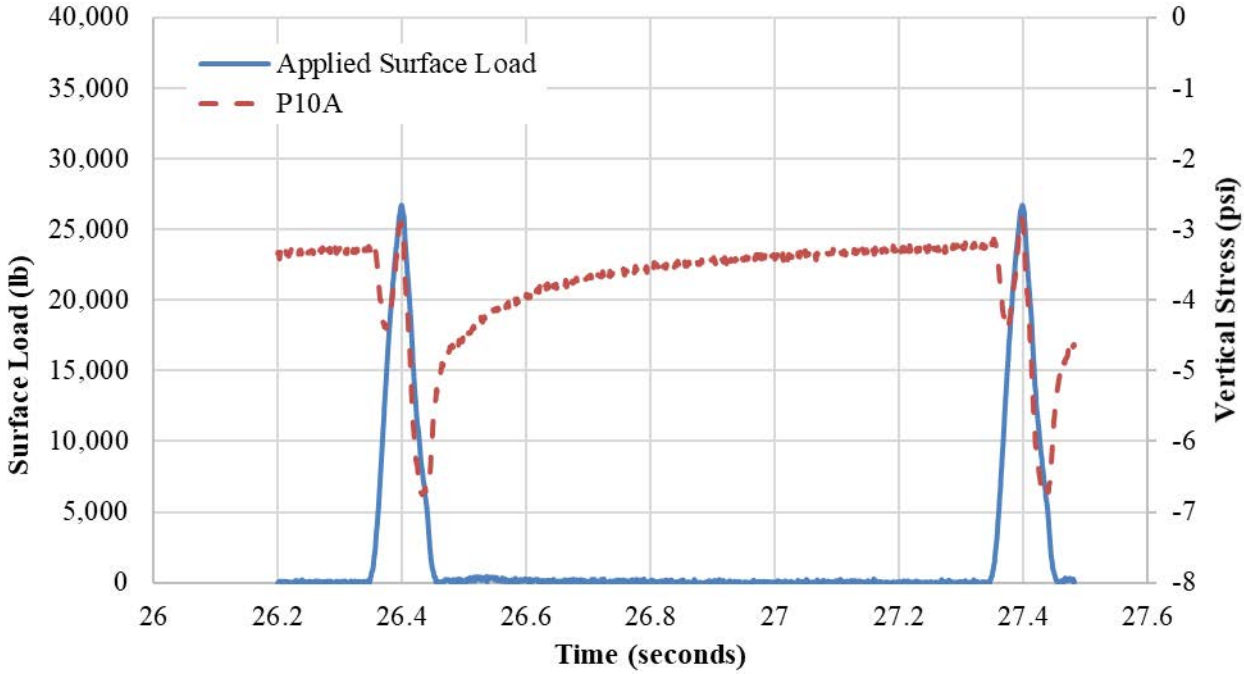




**Figure 58. Graph. One cycle of surface pulse load and stress response as recorded from P10A.**

### 3.3.4 Assessment of $SAF_{Flexible}$

As discussed in section 2.4, the presence of a flexible pipe buried under a full pavement structure will affect the stress distribution. None of the analytical methods were able to capture the vertical stress response as recorded by P10A, which was verified by the ovality check. Thus, an adjustment factor was needed to modify computed stresses to obtain the induced stresses. Since 3D-Move Analysis software can account for the material model for AC and CAB layers and is able to accurately capture the stress response without the presence of buried utilities (section 3.2), the computed stresses using 3D-Move Analysis software were used for the determination of $SAF_{Flexible}$.[10]

Figure 59 presents a comparison between measured and 3D-Move Analysis software-computed vertical stresses at the crown of the pipe. A linear trendline with zero intercept was imposed on both data sets to compute the slope. While a linear fitting may not necessarily fit the measured data, it represents a conservative approach.

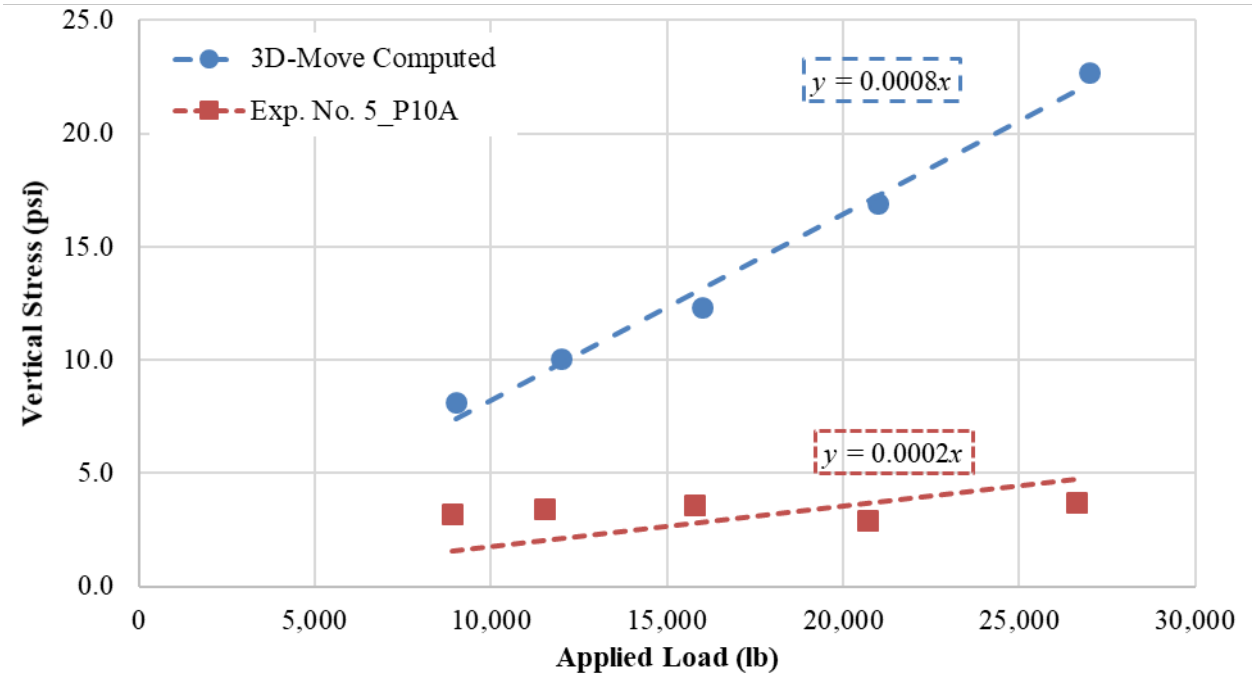




**Figure 59. Graph. Comparison between measured and 3D-Move Analysis software-computed stresses at the crown of the pipe.**

As indicated from the fitting equations in figure 59, 3D-Move Analysis software is more likely to estimate the vertical stresses about four times higher than the pipe is actually experiencing.[(10)] Thus, an adjustment factor of 0.25 should be expected. However, such a huge reduction in stress calculation cannot be recommended based solely on one experiment. More experiments are required to backup such a significant reduction. Thus, using an $SAF_{Flexible}$ value of 1 is recommended. The authors of this report recommend staying on the conservative side until further experimental testing and numerical investigations are carried out.

## 3.4. EXPERIMENTAL RESULTS AND OBSERVATIONS FOR RIGID CULVERT

In this section, the test results and observations obtained from experiment No. 5, when the surface loads were on the centerline of the rigid culvert, are presented.

### 3.4.1 Comparison of Pressure Cells

Figure 60 and figure 61 show the recorded vertical stresses measured by P10B and P1B in experiment No. 5 and P10 and P1 in experiment No. 3, respectively. All these TEPCs were located at the centerline of the surface FWD load. P10B and P10 were installed 6 inches from the SG surface, while P1B and P1 were placed 20 inches from the SG surface. P10B and P1B in experiment No. 5 were installed on the top and the bottom of the concrete culvert respectively, similar to the flexible pipe.

As presented in figure 60, the load-induced vertical stresses in experiment No. 5, measured by P10B, were higher than the measurements by P10 in experiment No. 3. However, substantially lower vertical stresses were measured by P1B compared to the measurements by P1, as shown in

figure 61. These observations can be attributed to the soil–structure interaction and higher rigidity (i.e., stiffness) of the concrete culvert with respect to the surrounding SG soil, revealing the need for the stress adjustment factor.

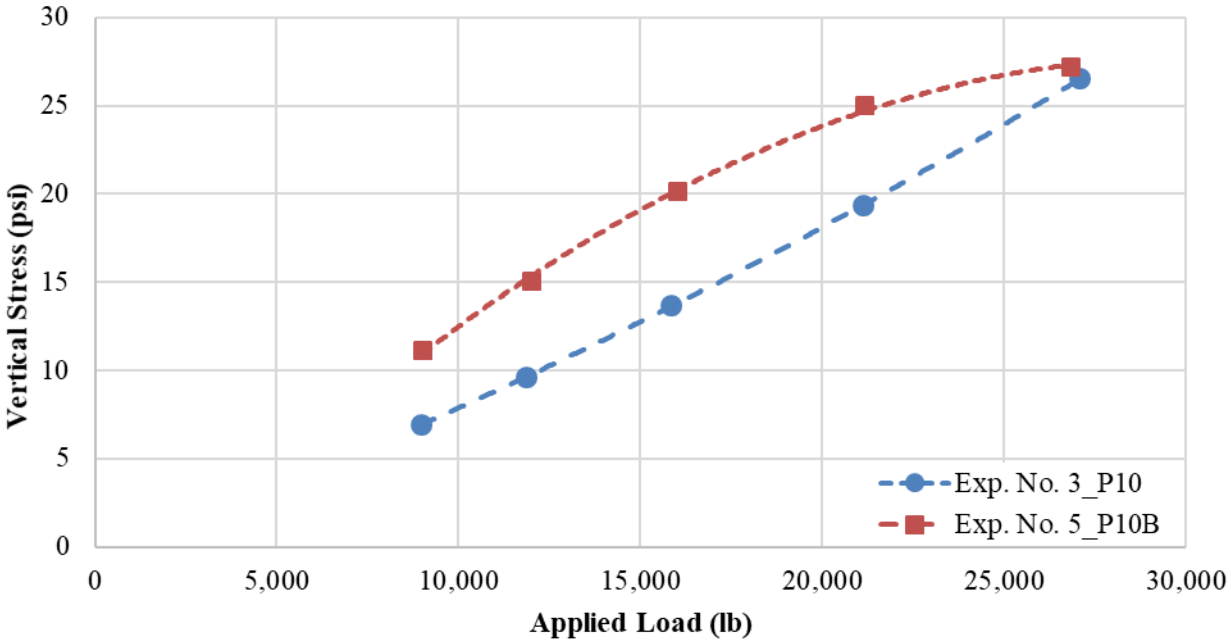




**Figure 60. Graph. Measured vertical stresses by P10 in experiment No. 3 and P10B in experiment No. 5.**

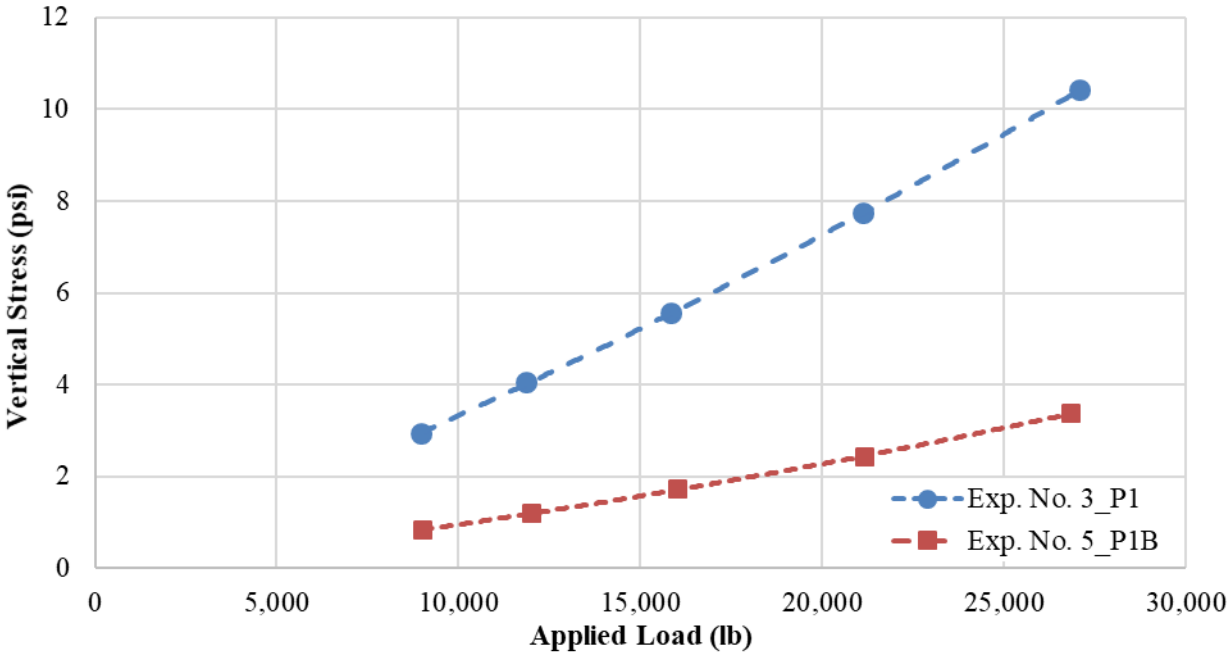




**Figure 61. Graph. Measured vertical stresses by P1 in experiment No. 3 and P1B in experiment No. 5.**

Figure 62 compares the measured vertical stresses on top of the culvert at the centerline of the load (P10B) obtained from experiment No. 5 and the calculated stresses using the AASHTO standard specification.[16] The estimated stresses were 75 percent higher on average than the measured values. These observations substantiate the need to consider AC and CAB layer stiffnesses when distribution of vertical stresses on top of culverts is to be determined. It should be noted that the box culvert was buried 17 inches below the AC surface.

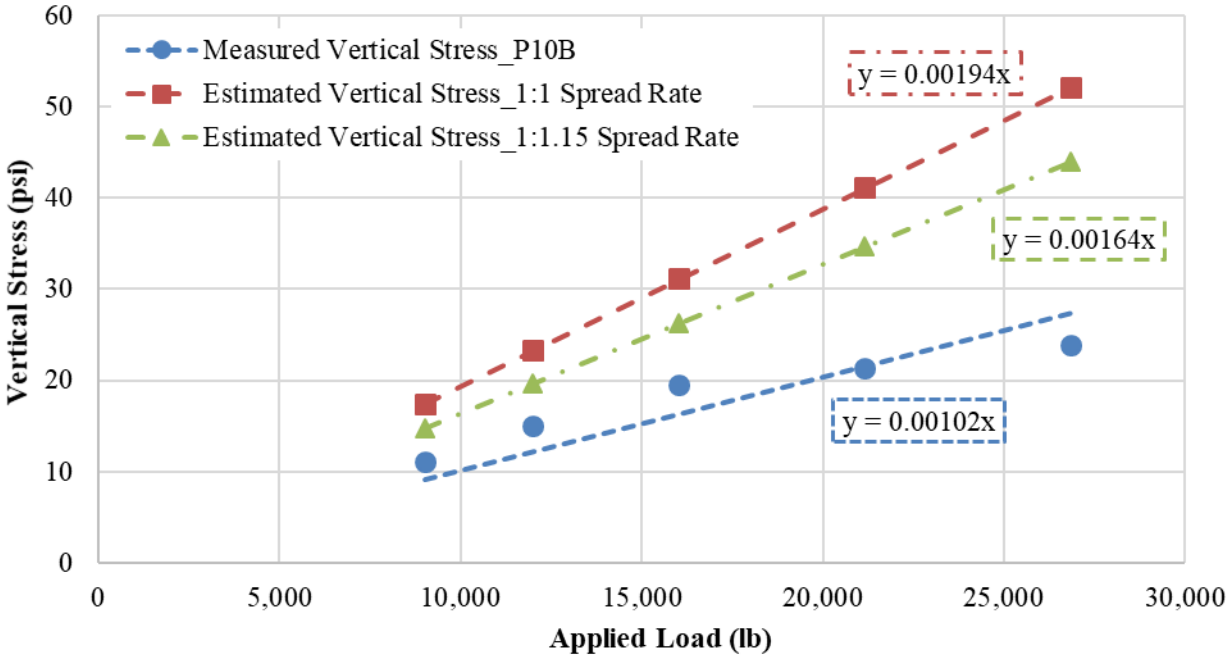




**Figure 62. Graph. Comparison between measured and estimated vertical stresses on top of the culvert in experiment No. 5.**

### 3.4.2 Assessment of $SAF_{Rigid}$

The determination of $SAF_{Rigid}$ is carried out by comparing the measured stresses in experiment No. 5 and the computed stresses using 3D-Move Analysis software.[10] The measured stresses in figure 63 reveal a nonlinear behavior with respect to the response of the rigid culvert, which may skew its trend line. To eliminate the error due to nonlinearity, the data were limited to a surface load of 21,000 lb, and the corresponding trend lines were used to determine $SAF_{Rigid}$.

Figure 64 presents the trend lines for measured and 3D-Move Analysis software-computed vertical stresses for a surface load up to 21,000 lb. As shown in the figure, by comparing the slope of the trend lines, measured vertical stresses on top of the box culvert were about 50 percent higher than those computed by 3D-Move Analysis software. According to these observations, an $SAF_{Rigid}$ value equal to 1.5 was recommended to be applied to the vertical stresses calculated using 3D-Move Analysis software.[10]

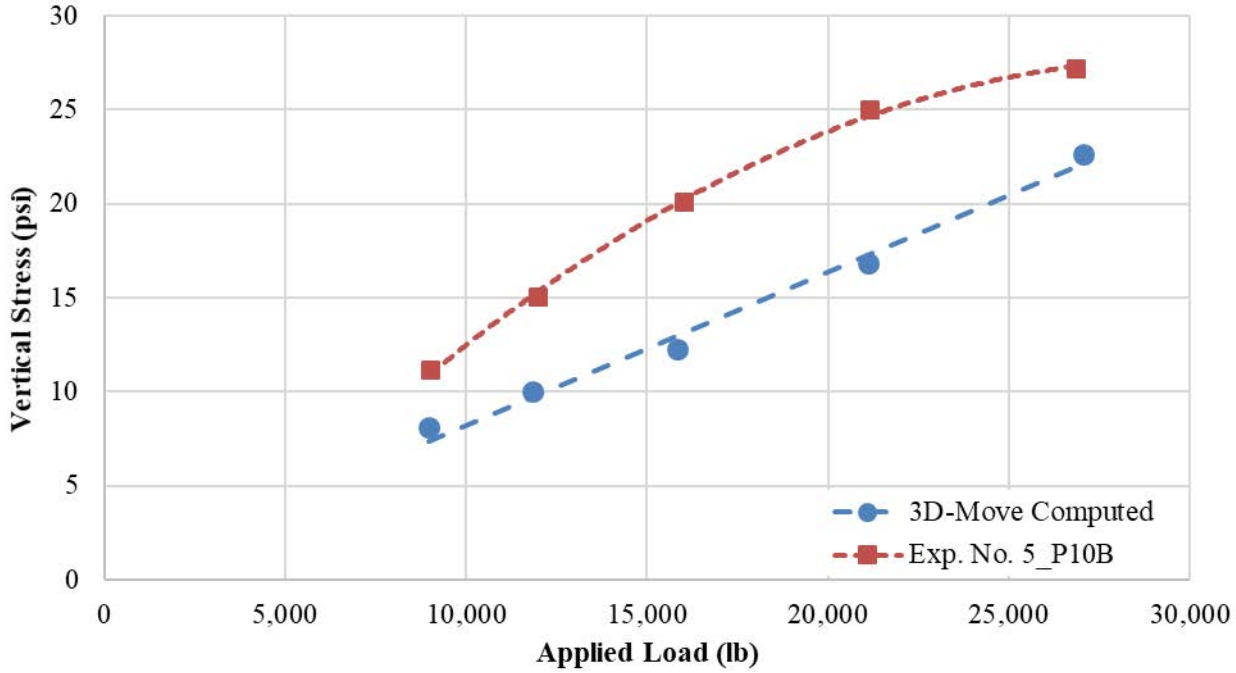




**Figure 63. Graph. Comparison between measured and 3D-Move Analysis software-computed stresses on top of the culvert.**

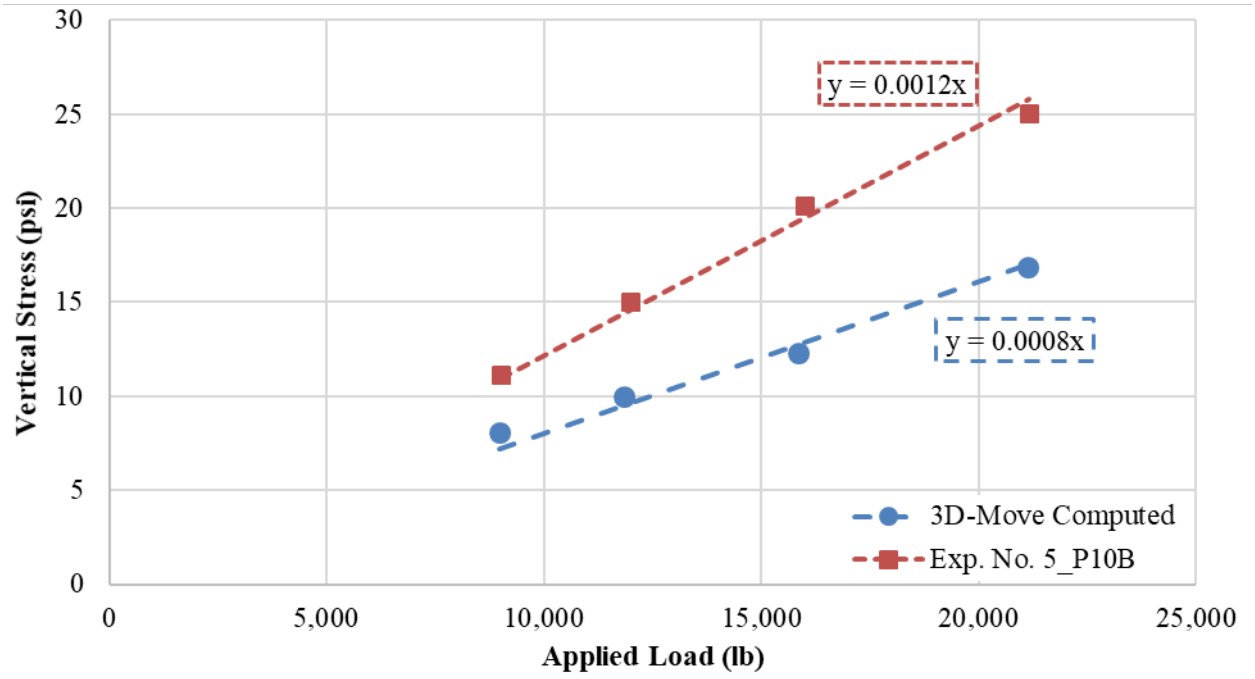




**Figure 64. Graph. Trend lines for measured and 3D-Move Analysis software-computed stresses on top of the culvert for a surface load.**

### 3.4.3 Structural Adequacy Analysis of Concrete Culvert in Experiment No. 5

To investigate the internal integrity of the buried concrete culvert in experiment No. 5, a structural analysis was conducted. The summary of required inputs for this exercise is presented in table 5. Figure 65 shows the computed stresses on top of the concrete culvert using 3D-Move Analysis software adjusted by an $SAF_{Rigid}$ value of 1.5.[10]

**Table 5. Inputs for structural adequacy analysis of concrete culvert in experiment No. 5.**

| Property | Value |
|---|---|
| AC unit weight (lb/ft$^3$) | 150 |
| Base unit weight (lb/ft$^3$) | 138 |
| SG unit weight (lb/ft$^3$) | 110 |
| SG angle of internal friction (degrees) | 38 |
| Top slab and bottom slab width (inches) | 12 |
| Top slab and bottom slab thickness (inches) | 1 |
| Sidewall height (inches) | 12 |
| Sidewall thickness (inches) | 1 |
| $D_{Reinforcement}$ (all members) (inches) | 0.15 |
| Spacing of longitudinal reinforcement (all members) (inches) | 4 |
| Diameter of shear reinforcement (all members) (inches) | 0.15 |
| $S_{shear}$ (all members) (inches) | 4 |
| Concrete cover on the reinforcements (all members) (inches) | 0.1 |
| $f'_c$ (psi) | 8,000 |
| $f_y$ (psi) | 80,000 |

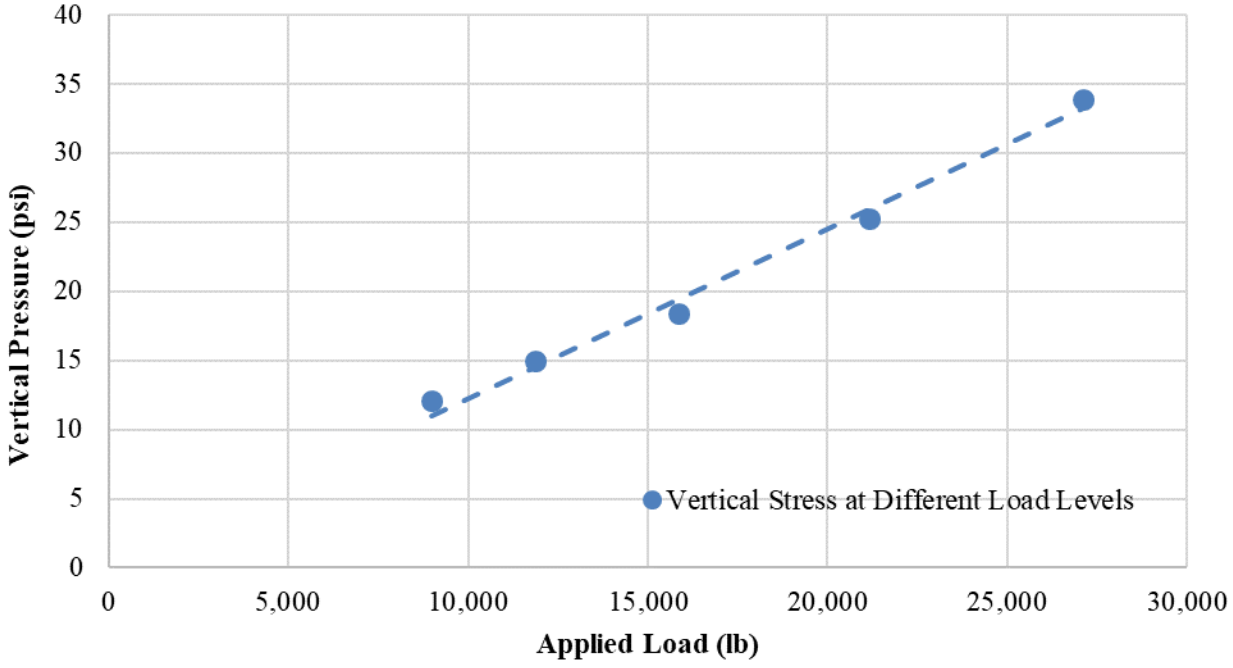




**Figure 65. Graph. Computed stress on top of the concrete culvert.**

Analyses of $M_u$, $V_u$, and $P_u$ for the members (i.e., top slab, bottom slab, and sidewalls) at different load levels are presented in table 6 through table 8, respectively. The concrete culvert is structurally adequate at all FWD load levels in terms of shear strength and $P_u$. However, at the highest FWD surface loading (i.e., 27,000 lb), $M_u$ in the members was higher than their flexural capacity (i.e., $\phi_f M_n$), which indicates a possibility of failure. Such an observation is consistent with the nonlinear behavior of rigid culvert response observed as skewness in the measured vertical stresses on top of the culvert at the highest FWD load level of 27,000 lb (figure 63). It should be noted that the concrete culvert was purposely designed in a way to experience distresses at the higher load levels of surface FWD loading.

**Table 6. $M_u$ investigation of concrete culvert in experiment No. 5.**

| Member | $\phi_f M_n$ (lb-inch) | $M_u$ at FWD Load of 8,971 lb (lb-inch) | $M_u$ at FWD Load of 11,857 lb (lb-inch) | $M_u$ at FWD Load of 15,860 lb (lb-inch) | $M_u$ at FWD Load of 21,146 lb (lb-inch) | $M_u$ at FWD Load of 27,087 lb (lb-inch) |
|---|---|---|---|---|---|---|
| Top slab | 3,011 | 1,486 | 1,791 | 2,163 | 2,900 | 3,832 |
| Bottom slab | 3,011 | 1,519 | 1,824 | 2,196 | 2,933 | 3,865 |
| Sidewall | 3,011 | 1,531 | 1,836 | 2,208 | 2,945 | 3,877 |

**Table 7. $V_u$ investigation of concrete culvert in experiment No. 5.**

| Member | $\phi_s V_n$ (lb) | $V_u$ at FWD Load of 8,971 lb (lb) | $V_u$ at FWD Load of 11,857 lb (lb) | $V_u$ at FWD Load of 15,860 lb (lb) | $V_u$ at FWD Load of 21,146 lb (lb) | $V_u$ at FWD Load of 27,087 lb (lb) |
|---|---|---|---|---|---|---|
| Top slab | 6,358 | 987 | 1,191 | 1,439 | 1,930 | 2,551 |
| Bottom slab | 6,358 | 1,007 | 1,211 | 1,459 | 1,950 | 2,571 |
| Sidewall | 6,358 | 512 | 614 | 738 | 983 | 1,294 |

**Table 8. $P_u$ investigation of concrete culvert in experiment No. 5.**

| Member | $\phi_a P_n$ (lb) | $P_u$ at FWD Load of 8,971 lb (lb) | $P_u$ at FWD Load of 11,857 lb (lb) | $P_u$ at FWD Load of 15,860 lb (lb) | $P_u$ at FWD Load of 21,146 lb (lb) | $P_u$ at FWD Load of 27,087 lb (lb) |
|---|---|---|---|---|---|---|
| Top slab | 7,535 | 497 | 599 | 723 | 968 | 1,280 |
| Bottom slab | 7,535 | 512 | 614 | 738 | 983 | 1,295 |
| Sidewall | 7,535 | 988 | 1,192 | 1,458 | 1,951 | 2,572 |

# CHAPTER 4. SUMMARY AND RECOMMENDATIONS

Developing a methodology to reliably analyze the risk of buried structures failure due to SHL movement on flexible pavements is one of the major components of this FHWA project. The methodology adopted in this study was based on widely accepted and available buried utility (flexible and rigid) design procedures.

For flexible pipes, a hybrid step-by-step evaluation procedure provided in the ALA and CEPA reports was implemented in this study.[19,20] The procedure is divided into four general checks: (1) assess $FOS_{CSF}$, (2) check $Pipe_{ovality}$ cross section, (3) check $\sigma_{crb}$, and (4) check $\sigma_{wc}$. On the other hand, in the case of a rigid concrete culvert, the stability is investigated by analyzing the $M_u$, $V_u$ and $P_u$ in the culvert members (i.e., top slab, bottom slab, and sidewalls) in accordance with the AASHTO standard specifications.[16]

However, a fair assessment of the induced stresses from dead (i.e., surcharge) and live (SHL vehicle) loads is required to analyze the internal integrity of a buried utility. Though the existing state-of-practice methodologies provide recommendations with respect to the load distribution, they are limited when assessing the risk to buried utilities under an SHL-vehicle movement. The significant shortfalls of the existing state of practice are considering only a standard truck (mostly HS20) as a live load, simulating it as a point load, rectangular loaded area, and applying the static load at the surface of unpaved roads (i.e., neglecting the AC and CAB layer).

Therefore, it was necessary to estimate the SHL-induced stresses using 3D-Move Analysis software to realistically simulate pavement structure and an SHL vehicle (e.g., viscoelastic properties of the AC layer and moving load). However, the software assumes uniform layers extending laterally to infinity without considering the role of soil–structure interaction and discontinuities within the medium (i.e., presence of buried utilities). To overcome this issue, a stress adjustment factor for buried utilities ($SAF_{Utility}$) is needed to modify the stresses computed using 3D-Move Analysis software at the location of the buried utility.[10]

In this study, $SAF_{Flexible}$ and $SAF_{Rigid}$ were determined based on the results obtained from two full-scale pavement structure experiments (with and without buried utilities). The control experiment represented a full pavement structure without any buried utilities subjected to surface FWD loads at different intensities. A similar pavement structure with two types of buried utilities installed in the SG was subjected to the same surface FWD loads applied directly above the centerlines of the buried utilities.

It was found that the vertical stresses experienced by the flexible pipe were much lower than those stresses transferred in the continuum medium (i.e., no buried utility). On the other hand, in the case of a concrete culvert, substantially higher vertical stresses were induced compared to those measured in the SG in the control experiment (i.e., no buried utility). In summary, using an $SAF_{Flexible}$ value of 1 is recommended. This recommendation is mainly on the conservative side until further experimental testing and numerical investigations are carried out. However, in the case of rigid culverts, an $SAF_{Rigid}$ value of 1.5 was recommended.

Additionally, further investigations of $SAF_{Utility}$ are recommended by conducting comprehensive experiments and additional numerical analyses. Such analyses should consider various scenarios of flexible pavement structures, depth of cover, buried utility dimensions and characteristics, etc., to cover other cases that were not considered as part of this study in the determination of $SAF_{Utility}$.

## REFERENCES


1. Hajj, E.Y., Siddharthan, R.V., Nabizadeh, H., Elfass, S., Nimeri, M., Kazemi, S.F., Batioja-Alvrez, D.D., and Piratheepan, M. (2018). *Analysis Procedures for Evaluating Superheavy Load Movement on Flexible Pavements, Volume I: Final Report*, Report No. FHWA-HRT-18-049, Federal Highway Administration, Washington, DC.

2. Nimeri, M., Nabizadeh, H., Hajj, E.Y., Siddharthan, R.V., Elfass, S, and Piratheepan, M. (2018). *Analysis Procedures for Evaluating Superheavy Load Movement on Flexible Pavements, Volume II: Appendix A, Experimental Program*, Report No. FHWA-HRT-18-050, Federal Highway Administration, Washington, DC.

3. Nimeri, M., Nabizadeh, H., Hajj, E.Y., Siddharthan, R.V., and Elfass, S. (2018). *Analysis Procedures for Evaluating Superheavy Load Movement on Flexible Pavements, Volume III: Appendix B, Superheavy Load Configurations and Nucleus of Analysis Vehicle*, Report No. FHWA-HRT-18-051, Federal Highway Administration, Washington, DC.

4. Nabizadeh, H., Hajj, E.Y., Siddharthan, R.V., and Elfass, S. (2018). *Analysis Procedures for Evaluating Superheavy Load Movement on Flexible Pavements, Volume IV: Appendix C, Material Characterization for Superheavy Load Movement Analysis*, Report No. FHWA-HRT-18-052, Federal Highway Administration, Washington, DC.

5. Nabizadeh, H., Hajj, E.Y., Siddharthan, R.V., Nimeri, M., Elfass, S., and Piratheepan, M. (2018). *Analysis Procedures for Evaluating Superheavy Load Movement on Flexible Pavements, Volume V: Appendix D, Estimation of Subgrade Shear Strength Parameters Using Falling Weight Deflectometer*, FHWA-HRT-18-053, Federal Highway Administration, Washington, DC.

6. Nabizadeh, H., Nimeri, M., Hajj, E.Y., Siddharthan, R.V., and Elfass, S. *(2018). Analysis Procedures for Evaluating Superheavy Load Movement on Flexible Pavements, Volume VI: Appendix E, Ultimate and Service Limit Analyses*, Report No. FHWA-HRT-18-054, Federal Highway Administration, Washington, DC.

7. Nabizadeh, H., Siddharthan, R.V., Elfass, S., and Hajj, E.Y. *(2018). Analysis Procedures for Evaluating Superheavy Load Movement on Flexible Pavements, Volume VII: Appendix F, Failure Analysis of Sloped Pavement Shoulders*, Report No. FHWA-HRT-18-055, Federal Highway Administration, Washington, DC.

8. Batioja-Alvarez, D.D., Hajj, E.Y., and Siddharthan, R.V. *(2018). Analysis Procedures for Evaluating Superheavy Load Movement on Flexible Pavements, Volume IX: Appendix H, Analysis of Cost Allocation Associated with Pavement Damage Under a Superheavy Load Vehicle Movement*, Report No. FHWA-HRT-18-057, Federal Highway Administration, Washington, DC.

9. Kazemi, S.F., Nabizadeh, H., Nimeri, M., Batioja-Alvarez, D.D., Hajj, E.Y., Siddharthan, R.V., and Hand, A.J.T. *(2019). Analysis Procedures for Evaluating Superheavy Load Movement on Flexible Pavements, Volume X: Appendix I, Analysis Package for Superheavy Load Vehicle*

*Movement on Flexible Pavement (SuperPACK),* Report No. FHWA-HRT-18-058, Federal Highway Administration, Washington, DC.

10. University of Nevada, Reno (2013). *3D-Move Analysis Software*, Version 2.1. Reno, NV. Available online at: http://www.arc.unr.edu/Software.html, last accessed September 19, 2017.

11. Moser, A.P. and Folkman, S. (2008). *Buried Pipe Design,* Third Edition, McGraw-Hill Companies, Inc., New York City, NY.

12. American Water Works Association. (2008). *Concrete Pressure Pipe*: *Manual of Water Supply Practices*, AWWA Manual M9, Third Edition, American Water Works Association, Denver, CO.

13. Marston, A. and Anderson, A.O. (1913). *The Theory of Loads on Pipes in Ditches, and Tests of Cement and Clay Drain Tile and Sewer Pipe, Bulletin No. 31*, Iowa State College of Agriculture and Mechanic Arts, Ames, IA.

14. Spangler, M.G. (1941). *The Structural Design of Flexible Pipe Culverts, Bulletin 153*, Iowa State College of Agriculture and Mechanic Arts, Ames, IA.

15. Petersen, D L., Nelson, C.R., Gang, L., McGrath, T.J., and Kitane, Y. (2010). *Recommended Design Specifications for Live Load Distribution to Buried Structures,* NCHRP Report No. 673, National Cooperative Highway Research Program, Washington, DC.

16. American Association of State Highway and Transportation Officials. (2012). *AASHTO LRFD Bridge Construction Specifications*, Sixth Edition, AASHTO, Washington, DC.

17. McGrath. T.J., Moore, I.D., Selig, E.T., Webb, M.C., and Taleb, B. *(2002). Recommended Specifications for Large-Span Culverts*, NCHRP Report No. 473, National Cooperative Highway Research Program, Washington, DC.

18. Kraus, E., Oh, J.H., Fernando, E., Li, E.Y., Quiroga, C., and Koncz, N. *(2011). Evaluating the Impact of Overweight Load Routing on Buried Utility Facilities*, Report No. FHWA/TX-11/0-6394-1, Texas Transportation Institute, College Station, TX.

19. American Lifelines Alliance. (2001). *Guidelines for the Design of Buried Steel Pipe*, American Society of Civil Engineering, Reston, VA.

20. Warman, D.J., Hart, J.D., and Francini, R.B. *(2009). Development of a Pipeline Surface Loading Screening Process and Assessment of Surface Load Dispersing Method*s, Report No. 05-44R1, Canadian Energy Pipeline Association, Worthington, OH.

21. American Petroleum Institute. (2007). *Steel Pipelines Crossing Railroads and Highways*, API RP 1102, American Petroleum Institute, Washington DC.

22. Fuerst, R.P., Robertson, S.T., and Bowles, L.M. (2013). *Method for Prediction of Flexible Pipe Deflection,* M-25, U.S. Department of the Interior Bureau of Reclamation, Washington, DC.

23. SAAP2000®. (2016). *Structural Software for Analysis and Design*, Version 18, Walnut Creek, CA.

24. BAKFAA. (2012). *Backcalculation Software*, Version 2.0, Federal Aviation Administration, Washington, DC.

25. Rohde, G.T. and Scullion, T. (1990). *MODULUS 4.0: Expansion and Validation of the MODULUS Backcalculation System*, Report No. FHWA/TX-91/1123-3, Texas Transportation Institute, College Station, TX.

HRDI-20/10-19(WEB)E